PCCP

Accepted Manuscript

ROYAL SOCIETY OF CHEMISTRY

www.rsc.org/pccp

Assessment of DFT Methods for Studying Acid Gases Capture by Ionic Liquids

Gregorio García,[a] Mert Atilhan,[b] Santiago Aparicio[*a]

[a] Department of Chemistry, University of Burgos, 09001 Burgos, Spain

[b] Department of Chemical Engineering, Qatar University, P.O. Box 2713, Doha, Qatar

[*]Corresponding author: e-mail: sapar@ubu.es

ABSTRACT

For the first time, this work reports an analysis on the performance of Density Functional methods for studying acid gases capture (CO_2 and SO_2) by ionic liquids (ILs). The considered functionals were selected as representatives of the available families: pure GGA (PBE and BLYP), hybrid (PBE0 and B3LYP), hybrid meta-GGA (M06, M06-2X and M06-HF), long range corrected (LC-PBEPBE, CAM-B3LYP, ωB97X) and dispersion corrected (PBE-D2, B3LYP-D2 and ωB97XD). Likewise, HF and MP2 were also applied. Binding energies of cation-anion interacting pairs as well as IL-CO_2 and IL-SO_2 systems were calculated for a set of 54 ILs and compared against MP2/aug-cc-pvDZ. Unlike previously reported DFT benchmarks on ILs, which calculated binding energies through single point calculations on fixed geometries, properties in this work were calculated for geometries optimized at each theoretical level. DFT functionals that are suitable for describing ion-ion and ion-gas interactions were identified, considering both coulombic forces and dispersion interactions. The reported results allowed to infer relationships to the rational design of ILs for acid gas capture.

KEYWORDS

Ionic liquids; carbon capture; acid gases; Density Functional Theory; benchmark.

Graphical Abstract

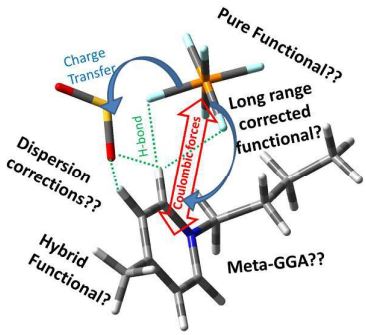

Acid Gas Capture by Ionic Liquids

1. INTRODUCTION

Ionic liquids (ILs) have emerged as a new generation of solvents because of their physicochemical properties, such as wide liquid range, high thermal and chemical stability, high ionic conductivity, non flammability or good solvent capabilities for organic, inorganic, organometalic and polymeric compounds. Nevertheless, the most important property of ILs is the possibility to design task-specific solvents, *i.e.*, the tuning of physicochemical properties through the suitable combination of ions.[1, 2] Such properties show ILs as potential solvents for their application in very different technologies such as lubrication, polymers, chemical synthesis or materials development. One of the most relevant applications of ILs is their use as solvents for acid gases adsorption and separation.[2, 3] Acid gases, such as carbon dioxide (CO_2) and sulfur dioxide (SO_2), are mainly emitted from fossil fuels combustion being the most relevant atmospheric pollutants, with a pivotal role in anthropogenic climate change.[4] At the same time, SO_2 is a useful source for many intermediates in chemical synthesis.[5] Therefore, there is a general interest in the design and improvement of suitable methods for CO_2 and SO_2 capture. The most common capturing technologies for acid gases capture are based on absorption with aqueous amine solutions,[6] which are also considered as reference methods in comparison with other alternatives.[7] Unfortunately, amine-based procedures have important drawbacks such as amine degradation,[8] equipment corrosion,[9] large energy consumption for solvent regeneration[10] and high operational costs,[11] which show the need of new technologies such as those based on ILs.

The design of ILs with improved features for gas acid capture needs a deep understanding on those factors governing absorption process and their relationship with the molecular structure. However, the larger number of possible ILs (~ 10^6 if only pure ILs are considered, which can be extended to ~ 10^{18} when mixed ILs are included) hinders to carry out systematic experimental studies. This is a context where molecular simulations are a powerful tool to provide a rational approach to a relevant technological problem, in this case for obtaining a molecular level description of acid gases adsorption by ionic liquids. Most of the literature dealing with acid gas capture by ILs using molecular simulations is mainly focused on the use of Molecular Dynamics (MD), which allows a realistic approach to macroscopic properties such as density, viscosity or diffusion coefficients as well as for the nanoscopic characterization of the adsorption mechanisms.[12-14] Regarding to molecular simulations based on Density Functional Theory (DFT), although effects such as long range interactions in ILs are despised, they provide a more direct knowledge at the molecular level on parameters such as charge distributions, binding energies or frontier molecular orbitals.

DFT studies on acid gas capture are mainly referred to CO_2,[13, 15-17] although some studies on SO_2 capture have also been reported.[16, 17] In both cases, most of them employ traditional B3LYP[18-20] functional along Pople's basis sets. At the molecular level, intermolecular interactions (cation-anion and ion-gas) are the key parameters related with acid gases capture using ILs. Although, anion-cation interactions are mainly driven by coulombic interactions, other interactions such as intermolecular hydrogen bonds between ions could be non-negligible and have strong effects on equilibrium geometries and related properties. DFT - based approach for studying intermolecular interaction in ILs have to be done with caution. For example, it is well known that dispersion interactions are poorly described using DFT methods,[21] or DFT generally overestimate charge transfer interactions.[22] Unfortunately, publications dealing with systematic applications of DFT and *ab initio* based methods to ILs are scarce.[23-27] Moreover, there are not studies on the systematic application of DFT methods (as well as *ab initio*) to acid gas capture by ILs. Therefore, a systematic study on the comparison of DFT and *ab initio* methods for acid gases capture by ILs is required. Gas adsorption at the molecular level is mainly carried out through dispersion interactions between ions and gas molecules, with anion$\cdots CO_2/SO_2$ interactions playing the main role.[13, 15-17] In addition, for anion$\cdots SO_2$ interactions there is a charge transfer between the anion specie and SO_2.[28] Thus, a systematic application of DFT methods to assess the main molecular parameters related with acid gas capture by ILs, *i.e.* cation-anion interactions and IL-CO_2/SO_2, is reported in this work. Several DFT methods based on pure, hybrid, hydrid meta-GGA, long range or empirical dispersion corrected functionals, as well as Moller-Plesset perturbation theory second-order (MP2)[29] and Hartree Fock (HF) methods have been applied. For this purpose, a set of 54 ILs (Fig. 1 and Table 1), which are expected to provide high acid gases solubility, has been selected according to a previous study using B3LYP functional.[30] The reported results have allowed to obtain information on the functionals suitability for describing anion$\cdots$cation interactions, extending the number of considered functionals previously analyzed by Izgorodina, Zahn, Grimme *et al.*,[23-27] and for those properties related with acid gases capture for the first time.

2. METHODS

2.1. DFT and *Ab Initio* Methods. All theoretical methods here described have been applied as implemented in Gaussian 09 (Rev. D01) package.[31] In this work, selected DFT methods span the gamut of modern functionals, which could be classified in at least five large families:

i) *Pure GGA functionals with 0% HF exchange*: PBE[32] and BLYP,[18, 20] which are among the most common pure GGA functionals.[21] One of the main characteristic of PBE functional is the absence of empirical parameters.[32]

ii) *Hybrid functionals*, which include some % HF exchange into the functional. In this group we have selected B3LYP[18-20] and PBE0[33] (also known as PBE1PBE) functionals. B3LYP (20% HF exchange) is a three parameters functional, which shares the same correlation expression[18] and part of the exchange functional[20] than BLYP. Although this functional is widely employed, its good applicability is derived of some cancelation of errors.[21] PBE0 functional is obtaining from PBE functional taking into account a 25% of HF exchange. PBE0 is also empirical parameters free.

iii) *Meta-GGA functionals*. GGA functionals (pure or hybrid) only includes the density and its first derivative in the exchange-correlation potential, while meta-GGA functionals also incorporate the Laplacian (second derivative) of the density or the kinetic energy density. In turn, meta-GGA functional can be pure meta-GGA or hybrid meta-GGA.[34] These functionals are parameterized some extent according with experimental data.[21] Truhlar *et al.* have developed several functionals (e.g. M05-class and M06-class) with improved accuracy over popular B3LYP functional.[34] M06, M06-2X and M06-HF hybrid meta-GGA functionals, which have 27%, 54% and 100 % HF exchange, respectively,[34-36] were selected in this work. These functionals show promising performance for non-covalent interactions.[35] In the case of M06-2X functional, the "medium-range" electron correlation would be enough for describing the dispersion interactions in systems near their equilibrium geometries.[35]

As said, dispersion forces (such as hydrogen bonds or van der Waals interactions) play a key role for ion-ion and ion$\cdots CO_2/SO_2$ interactions. Anion-cation and anion$\cdots SO_2$ charge transfers are also important parameters. DFT methods do not describe dispersion interactions properly,[21] and charge transfer interactions tend to be overstimated.[22] Likewise, the importance of van der Waals forces in providing the correct qualitative description of charge-transfer interactions has been reported,[37] but the suitability of different DFT methods for describing charge transfer in ILs has not been studied in the literature. Nonetheless, it is well known that charge transfer processes in ionic compounds are strongly affected by self-interaction errors (SIE) due to artificial charge transfer from the anion to the cation.[38] SIE is derived from a qualitatively incorrect asymptotic potential description for the exchange

correlation functional.[21] In this sense, M06-HF has a full HF exchange, which eliminates SIE at long range.[36]

iv) *Long Range Corrected* (LRC) functionals minimize the SIE through the splitting of the Coulomb repulsion energy into long-range and short-range terms.[39] LC-PBEPBE and CAM-B3LYP functionals were selected, which allowed to obtain information on long range correction effects on pure (PBE) and hydrid functionals (B3LYP). LC-PBEPBE is obtained from PBE functional through the long range correction of Hirao *et al*.,[40] while CAM-B3LYP is a long range corrected version of B3LYP using the Coulomb-attenuating method.[41] ωB97X[42] functional was also chosen because it considers a small fraction of the short range HF exchange, as well as long range corrections, leading to improved accuracy in thermochemistry, kinetic and non-covalent interactions in comparison with common hybrid density functionals.[42]

v) *Dispersion corrected functionals*. Although there are several approximations, the most common approach is based on force field potentials developed by Grimme,[43] with the form $V_{ij}(R) = -C_{6,ij}f_{d,ij}(R)/R^6$, for two atoms *i* and *j* at a distance *R*, whose coefficients $C_{6,ij}$ rely on atomic polarizability data. The damping function, $f_{d,ij}(R)$, minimizes double counting of "short range" correlation effects captured by the density functional. Among the schemes developed by Grimme, D2-approach (DFT-D2)[43] is used in this work. Thus, PBE-D2 and B3LYP-D2 functionals, obtained by applying D2-approach on PBE and B3LYP functionals, were selected. ωB97XD,[44] which is a re-optimization of ωB97X functional to include dispersion corrections according to D2-approach, was also employed. Thus, information about dispersion effects (D2) on different kind of functionals, *i.e.* pure, hybrid and LRC, may be inferred. Further, calculated energies after dispersion corrections are comparable with more reliable values, such as those obtained at MP2 level.[45] In addition to D2 approach, Grimme *et al*. have also developed other improved dispersion correction schemes, commonly known as D3[46] or D3BJ.[47] Both approaches are available for PBE and B3LYP functionals, as well as ωB97X-D3 functional has been developed by Lin *et al.*[48] Unfortunately, ωB97X-D3 functional is not available Gaussian 09 (Revision D.01) package, so we selected D2 scheme for pure, hybrid and LRC functionals.

The selected functionals are representative of most families of currently adopted functionals. Double Hybrid (DH) functionals incorporate the correlation energy as a

perturbation term computed at MP2 level. Based on PBE0 and B3LYP functional, PBE0-DH[49] and B2PLYP-DH[50] have being extensively studied in the literature. Nevertheless, Adamo *et al.* showed that the behavior of both DH functionals is parallel to the corresponding hybrid ones,[51] but at a higher computational cost (due to MP2 contribution), and thus, they were not considered in this work.

HF and MP2 methods were also considered. MP2 is a good alternative to high correlated methods for studying non-convalent interactions, outperforming many DFT methods. MP2 describes intermolecular interactions in ILs with similar accuracy than coupled cluster calculations (e. g. CCSD).[23, 52, 53] High level calculations (such as CCSD) with a complete basis sets would be the best option as reference methods. Nonetheless, the application of coupler cluster theory with a moderate computational cost is only limited to small molecular systems. As matter of fact, the high computational cost required for CCSD calculations leads to scarce studies of ILs, which are mainly limited to imidazolium based ILs.[23, 25, 54] For instance, Izgorodina *et al.*,[24] applied CCSD calculations to small ionic liquids containing over 12 non-hydrogen atoms, which allowed the use of CCSD as benchmark method with a moderate computational cost. The available information shows that MP2 could provide a suitable reference data, without considerable deviation from CCSD, but at a lower computational cost, to study non covalent interactions.[45, 52, 55]. In fact, Tsuzuki *et al.* shown that MP2 lead to similar accuracy that CCSD(T) for studying intermolecular interactions in ionic liquids.[56] For the sake of the computational cost (in this paper a great effort has been invested in optimizing molecular geometries at each theoretical level), MP2 method in combination with aug-cc-pvDZ basis set was established as reference method. Even though, some calculations were carried out at CCSD/aug-cc-pvTZ theoretical level for [EMIM][BF4] ionic liquids (IL 1) as well as their complexes with CO_2 and SO_2 gases, whose binding energies were computed as described below. For IL 1, obtained results at MP2/aug-cc-pvDZ are in good agreement with values computed at CCSD/aug-cc-pvTZ, leading to energy deviation not larger than 3.9% Kcal mol^{-1}.

Basis set should also have a relevant role in calculated properties, the use of incomplete basis sets will not reflect the performance of selected method.[57] As said, this work main pursues to assess the performance of selected functionals, and thus, only few basis, including polarization and diffuse functions, were chosen aimed at obtaining some information about basis set effects: 6-31G*, 6-31+G**, 6-311+G** and aug-cc-pvDZ basis set. The latter could be considered the highest quality basis set.

2.2. Computational Protocol. All DFT, HF and MP2 calculations were done using Gaussian 09 (Revision D.01) package. Firstly, all studied systems (those composed by one isolated molecule, *i.e.* isolated ions, CO_2 and SO_2, as well as those composed by both ions and one acid gas molecule) were optimized at B3LYP/6-31G* level. For isolated ions, previously to the optimization, we have carried out (when needed) a conformational search based on the torsional barriers around chemical bonds. For those simulations wherein two or more molecules are present, different starting points were considered for studying different relative arrangements, but the study was limited to the configuration of minimal energy. Once identified the structures of minimal energy, they were confirmed as a real minimum through their vibrational frequencies. All systems were re-optimized at PBE, BLYP, PBE0, B3LYP, LC-PBEPBE, CAM-B3LYP, ωB97X, PBEPBE-D2, B3LYP-D2, ωB97XD, M06, M06-2X, M06-HF and HF in combination with 6-31G*, 6-31+G**, 6-311+G** and aug-cc-pvDZ basis sets. Iodine atoms were described through a small core Stuttgart-Dresden-Bonn effective core potential (SDB-cc-pVTZ).[58] Previously reported DFT benchmarks on ILs are based on SP calculations over fixing geometries,[23-25, 27] this approach could be very useful to asses energy-related changes derived from the selected functional, avoiding geometrical effects. However, the ability of the functional to provide suitable geometries is not tested. Most of the computational effort required in the calculation is used in the optimization process, and thus, to reduce the high computational cost derived from MP2 calculations, only SP were done for MP2/basis over B3LYP/basis optimized geometries.

The performance of DFT methods has been mainly evaluated through the binding energy (ΔE), which is defined as the energy difference between the energy sum of the different monomers and the total energy of the cluster system. Therefore, binding energy for ILs pairs was estimated as:

$$\Delta E_{IL} = (E_{cat} + E_{ani}) - E_{IL} \quad (1)$$

where E_{IL}, E_{cat} and E_{ani} stand for the energies of ILs pairs (anion plus cation complex), cation and anion, respectively. For IL···CO_2/SO_2 complexes, the binding energies were calculated in two ways; i) according to eq. 2:

$$\Delta E_{cat\text{-}ani\text{-}CO2} = (E_{cat} + E_{ani} + E_{CO2}) - E_{IL\text{-}CO2} \quad (2)$$

where the coulombic interaction between ions is the largest contribution; ii) Considering the IL as a whole, eq. 3:

$$\Delta E_{IL\text{-}CO2} = (E_{IL} + E_{CO2}) - E_{IL\text{-}CO2} \quad (3)$$

where $E_{IL\text{-}CO2}$ and E_{CO2} are the energies for IL-CO_2 and CO_2 systems, respectively. The latter allows a direct comparison between different ionic liquids regardless of the strength of the

coulombic interaction between ions. Basis set superposition error (BSSE) was considered for all the calculated energies, which were corrected according to counterpoise method.[59]

3. RESULS AND DISCUSSIONS

A total of 60 method/basis set combinations have been evaluated through the analysis of binding energies of isolated 54 ionic liquids, 36 cation-XO_2 (XO_2 = CO_2, SO_2), 32 anion-XO_2 and 108 IL-XO_2 systems. From these data, root-mean square deviations (RMSD) with respect to MP2/aug-cc-pvDZ theoretical level were calculated. The discussion is divided into three sections aimed to assess the performance of selected DFT methods on the study of acid gases capture (CO_2 and SO_2) by ionic liquids. The first and second sections provide a detailed analysis of the effects of selected DFT method on the predicted cation···anion and IL···CO_2/SO_2 binding energies, with binding energies at each theoretical level were computed using the corresponding structures optimized at the same level. Hence, energy deviations can be also influenced by geometrical factors, and thus, DFT effects on optimized geometries have been also discussed paying attention on the intermolecular distances corresponding to the main interaction between ions, or between ions and gas molecules. The last section reports an insight into the relationship of IL-CO_2/SO_2 binding energies with anion-cation and ion-CO_2/SO_2 as well as the capability of selected ILs as acid gas capture agents based on binding energies.

3.1. Cation···Anion Interactions in Ionic Liquids. Studies on the performance of DFT methods for describing cation···anion interactions in ILs are scarce in the literature. Zahn *et al.*[26] performed a comparison between several functionals (including two D2-corrected functionals) and MP2 method for [BMIM][DCA] (IL 45 in our paper). Compared with standard functionals, dispersion corrected functionals led to an improvement of the results, reducing the mean absolute deviation to less than 2.5 Kcal mol^{-1}. Izgorodina *et al.*[24] carried out a similar study (although also including more recent DFT methods such as M05 or M05-2X) for pyrrolidinium based ionic liquids paired with anions such as $[Cl]^-$, $[BF4]^-$, $[PF_6]$ or $[SO_3CF_3]$. These authors advanced in their previous studies considering a larger number of ILs as well as DFT methods, including DH functionals, showing suitable performance of dispersion corrected functionals when compared with CCSD calculations, and DH functionals behaving similarly to GGA methods.[25] Grimme *et al.*[27] used standard hybrid, GGA and dispersion-corrected (D3BJ) functionals according to Grimme's method but also these authors considered non-local van der Waals functionals on ILs based on imidazolium and alkyl-phosponium cations with $[Cl]^-$, $[DCA]^-$ and acetate anions.[27] The analysis of the

available literature information shows that dispersion-corrected functionals are the most suitable option for studying cation-anion interactions in ILs. Nevertheless, all the available studies considered binding energies estimated over fixed geometries (generally optimized at B3LYP level), which does not allow to infer the advantages (or disadvantages) of studied functionals for the prediction of equilibrium geometries. Likewise, it is known that standard DFT methods fail due to SIE but any of the available studies have tested long range corrected functionals, which minimize the SIE.

The set of 54 ILs was selected because of expected high acid gases solubilities (Fig. 1 and Table 1),[30] and thus, the considered ILs allow the study of DFT performance on different types of ILs beyond classical ILs such as imidazolium-based ones. The studied set contains cations such as imidazolium, pyridinium, piperazinium, cholinium, ethylamonium or triethylsulfonion paired with $[BF_4]^-$, $[PF_6]^-$, $[NTf_2]^-$, diacianamide, triflate, phosphate, sulfate, thiocianate or halide anions. The average value of cation-anion binding energies ($\Delta E_{IL,av}$) at each theoretical level is reported in Fig. 2a. Binding energies are in the 77.08 Kcal mol^{-1} (for BLYP/6-31+G*) to 89.54 Kcal mol^{-1} (for M06HF/aug-cc-pvDZ) range. The results in Fig. 2b show that all selected theoretical levels leads to suitable accuracy against MP2/ aug-cc-pvDZ binding energies. Except M06HF/aug-cc-pvDZ level, all selected functionals yields RMSD $\simeq$ 0.70 Kcal mol^{-1}. In particular, the lowest RMSD are obtained for LRC functional independently of the selected basis set. LRC functionals present a variable percentage of HF contribution, which should be useful for an improvement of the description of charge transfer process from the anion to the cation but the reported results show that increasing HF contribution does not lead to smaller error. B3LYP (20% HF) and PBE0 (25% HF) yield similar $\Delta E_{IL,av}$ and RMSD values in comparison with pure BLYP and PBE functionals. Likewise, the increasing HF contribution of M06, M062X and M06HF functionals (from 27% up to 100%) only has slight effects on RMSD values. Literature studies[24-27] have showed that dispersion-corrected functionals lead to small deviations in comparison with reference data. However, the use of D2 approach with PBE and B3LYP functionals increases RMSD deviations. This is confirmed in this work where for example RMSD = 0.65 Kcal mol^{-1} for B3LYP/6-31+G* and RMSD = 0.83 Kcal mol^{-1} for B3LYP-D2/6-31+G* are obtained. The analysis of the optimized structures associated with PBE -PBE-D2 and B3LYP - B3LYP-D2 functionals revealed a slight shortening of the intermolecular distances such as hydrogen bonds, which in addition to the dispersion energy due to D2-approach leads to an increase of the binding energy. ωB97XD is a LRC functional that incorporates D2 correction, but the computed cation-anion binding energies and RMSD using ωB97XD are similar to those

estimated with ωB97X functional. It can be concluded that LRC funcionals provide the best performance to describe cation-anion interactions. In addition, long range correction in ωB97XD functional is able of correcting over-estimated binding energies due to shortened intermolecular dispersion interactions. This functional provides an adequate description of charge transfer process in ILs even in combination with modest Pople's basis sets, which provides a good choice for studying ILs.

A detailed analysis of the largest deviations with reference data at M06HF/aug-cc-PVDZ level reveals that charge transfer between ions (according ChelpG method[60]) in ILs 35-39 (which are based on imidazolium cations paired with $[SO_3CF_3]^-$) is overestimated according with charge transfer estimated at MP2/aug-cc-PVDZ theoretical level.

The effect of theoretical level on optimized geometries is reported in Fig. 2c. For simplifying purposes, the analysis is limited to the shortest distances between ions. RMSD deviations were calculated considering the sum of the corresponding van der Waals radii as reference values. For example, for IL 1 ([EMIM][BF_4]), the shortest distance between both atoms (instead of the selected methods) is always those one between H atom at position 2 of imidazol cation and one F atom of tetrafluoroborate atom. In this case, the sum of van-der Waals radii (2.55 Å) of both H (1.20 Å) and F (1.35 Å) was used as reference. It was found that all measured distances are smaller than the sum of van-der Waals radii, thus large / low RMSD deviations correspond to short / large intermolecular distances between ions. Overall, 6-31G* and aug-cc-PVDZ basis set perform larger RMSD than 6-31+G** or 6-311+G** basis sets. PBE / B3LYP functional in combination with 6-31+G** basis set led to RMSD = 0.084 Å / 0.083 Å. The inclusion of dispersion corrections (PBE-D2 / B3LYP-D2) yielded RMSD = 0.082 Å / 0.076 Å, while RMSD = 0.079 Å / 0.080 Å for LC-PBEPBE / CAM-B3LYP functionals. Both long range and dispersion corrections led to shortened anion-cation distances. Although LRC functionals provide a similar description on the intermolecular interactions in comparison with dispersion corrected ones, their improved charge transfer description led to lower energy deviations. Although the inclusion of D2 approach in ωB97XD also resulted in shorter intermolecular distances, changes on energy deviations and intermolecular distances are not inferred in comparison with ωB97X. Therefore, a good charge-transfer description plays a more important role than an adequate description of dispersion interactions when analyzing anion-cation pairs.

3.2. Ion···CO_2/SO_2 Interactions. The analysis of ion··· CO_2/SO_2 binding energies was carried out for rationalizing the behavior of IL···CO_2/SO_2 systems. Figures 3 and 4 collect average values of cation-CO_2 and cation-SO_2 binding energies ($\Delta E_{cat\text{-}CO2,av}$, $\Delta E_{cat\text{-}SO2,av,}$) and

RMSD deviations in comparison with MP2/aug-cc-pvDZ theoretical level. For cation-CO_2/ anion-SO_2 systems binding energies between 2.51 Kcal mol^{-1} (at BLYP/6-31+G**) and 4.85 Kcal mol^{-1} (at B3LYP-D2/aug-cc-pvDZ)/ 5.57 Kcal mol^{-1} (at BLYP/6-31+G**) and 9.87 Kcal mol^{-1} (at B3LYP-D2/aug-cc-pvDZ) were obtained. These values are in agreement with weak cation-gas interactions.[16] $\Delta E_{cat\text{-}CO2,av}$, $\Delta E_{cat\text{-}SO2,av}$ follow the same trend as a function of the theoretical level. In general, hybrid meta-GGA (M06, M06-2X and M06-HF) and dispersion corrected functionals as well (PBE-D2, B3LYP-D2 and ωB97XD) provide the largest deviations against MP2/aug-cc-pvDZ reference level, whereas the smallest RMSD values are obtained by using CAM-B3LYP and LC-PBEPBE functionals.

For cation-CO_2 systems, most of the selected functionals provide RMSD in the 0.15 Kcal mol^{-1} to 0.20 Kcal mol^{-1} range, regardless of the selected basis set. The percentage of HF contribution has different effects as a function of the selected functional. For instance, PBE / BLYP functionals in combination with 6-31+G** yield RMSD = 0.14 Kcal mol^{-1}/ 0.38 Kcal mol^{-1}, with negligible effect of the basis set, whereas both PBE0 and B3LYP functionals leads to RMSD $\simeq$ 0.20 Kcal mol^{-1}. The increasing HF percentage in selected hybrid meta-GGA functionals has minor effects on RMSD values, which increase from 0.15 Kcal mol^{-1} (M06/6-31+G**) to 0.23 Kcal mol^{-1} (M06-HF/6-31+G**). LC-PBEPBE and CAM-B3LYP offer the worst choice for estimating binding energies of cation-CO_2 systems (RMSD $\simeq$ 0.36 Kcal mol^{-1}). However, RMSD deviations calculated using ωB97X functional are roughly 0.18 Kcal mol^{-1}. In general, the inclusion of D2-approach allows a slight improvement of RMSD values. RMSD changed from 0.14 Kcal mol^{-1} (PBE/6-31+G**) / 0.20 Kcal mol^{-1} (at B3LYP/6-31+G** level)/ 0.18 Kcal mol^{-1} (at ωB97X /6-31+G** level) to 0.16 Kcal mol^{-1} (PBE/6-31+G**) / 0.16 Kcal mol^{-1} (B3LYP/6-31+G**) / 0.16 Kcal mol^{-1} (ωB97X /6-31+G**). Cation-CO_2 interactions are mainly driven by dispersion-forces, and thus, dispersion corrected functionals would be the best option for studying cation-CO_2 systems. As previously noted, ωB97X and ωB97XD functionals are the less affected by the basis set election.

RMSD for cation-SO_2 systems follow the same qualitative trends than cation-CO_2 ones, but cation-SO_2 values are more affected by the selected basis set. The largest deviations for binding energies of cation-SO_2 systems are obtained by using BLYP functional, where considering HF contribution (B3LYP) allows an improvement on estimated cation-SO_2 binding energies. Corrected dispersion functionals (PBE-D2, B3LYP-D2 and ωB97XD) provide worse results (RMSD $\simeq$ 0.28 Kcal mol^{-1}) than their corresponding uncorrected dispersion partners (RMSD $\simeq$ 0.30 Kcal mol^{-1}).

The results obtained from anion-CO_2 and anion-SO_2 systems are displayed in Figures 5 ($\Delta E_{ani\text{-}CO2,av}$, $\Delta E_{ani\text{-}SO2,av}$) and 6 (RMSD). In the analysis of anion-XO_2 interactions, it should be remarked their prevailing role for acid gases capture.[13, 15-17] The studied anions provide larger gas affinities than the considered cations. The mechanism of anion-XO_2 interaction is characterized by dispersion forces but also by charge transfer from the anion to the gas molecule, due to their acid character. This charge transfer is stronger for SO_2 than for CO_2 and proportional to the anion basicity, playing an important role on gas adsorption capacity.[28] CO_2 and SO_2 molecules do not follow the same pattern with regard to the applied theoretical level. For anion-CO_2, RMSD $\leq$ 0.80 Kcal mol^{-1} for PBE, B3LYP, PBE0, B3LYP, M06, LRC and dispersion corrected (as well as HF method) functionals. The increasing % HF for hybrid meta-GGA family (M06, M06-2X and M06-HF) leads to an increment of the RMSD from 0.71 Kcal mol^{-1} to 1.29 Kcal mol^{-1} (using 6-31+G** basis set). LRC functionals provide RMSD $\simeq$ 0.80 Kcal mol^{-1}, except LC-PBEPBE for which RMSD = 0.48 Kcal mol^{-1}. For PBE and B3LYP, the inclusion of dispersion corrections leads to less accurate description of ion-CO_2 binding energies. However, ωB97XD functional yields RMSD = 0.48 Kcal mol^{-1}.

Regarding to anion-SO_2 binding energies, the largest RMSD are obtained at M06-HF/aug-cc-pvDZ, which is due to an overestimation of charge transfer from triflate anion. LC-PBEPBE functional provides the lowest RMSD with regard to MP2 method, and the inclusion of dispersion terms in ωB97XD also leads to improved RMSD values. Hence, long range corrections as implemented in LC-PBEPBE and ωB97X functionals are needed for a good description on anion-SO_2 systems, mainly due to the presence of charge transfer process. Nevertheless, functionals with high % HF contribution (hybrid meta-GGA functionals) do not provide a good description of charge transfer process. Likewise, although ωB97XD functional does not lead to the lowest RMSD, the inclusion of long range and dispersion corrections improve standard hybrid functionals.

The performance of selected DFT methods for predicting ion-gas binding energies was studied considering RMSD values for a set composed by all ion-gas systems, *i.e.*, 18 cation-CO_2 + 18-cation-SO_2 + 16 anion-CO_2 + 16-anion-SO_2 (Fig. 7). The profiles reported in this Figure are mainly driven by anion-SO_2 interactions. ωB97XD functional provides lower RMSD values than standard hybrid functionals, whereas its performance is only improved by LC-PBEPBE functional. In our opinion, ωB97XD functionals brings together two essential requirements for an adequate description of the studied ion-gas systems: *i*) D2 approach for the description of cation-gas interactions (mainly driven by weak dispersion interactions), and *ii*) long range correction for describing charge transfer process (also present in anion-gas

systems). Moreover, long range corrections also led to a suitable description of cation-anion interactions. Therefore, previously to study IL-gas systems, ωB97XD with any basis set is a suitable option for studying CO_2/SO_2 capture by ionic liquids.

3.3. Ionic Liquid···CO_2/SO_2 Interactions. Binding energies of IL-XO_2 systems were estimated through eqs. 1 and 2 ($\Delta E_{cat\text{-}ani\text{-}XO2}$ and $\Delta E_{IL\text{-}XO2}$, respectively). Figures 8/10 and 9/11 collect average values of IL-XO_2 binding energies according to eq. 2 ($\Delta E_{cat\text{-}ani\text{-}XO2,av}$) /eq. 3 ($\Delta E_{IL\text{-}XO2,av}$) and their RMSD against MP2/aug-cc-pvDZ level. Regarding to $\Delta E_{cat\text{-}ani\text{-}XO2,av}$, this binding energy has three contributions: cation-anion, cation-gas and anion-gas interactions, with the largest contribution rising from cation-anion interactions but ion-gas interactions play the main role in the gas adsorption process.[13, 15-17] Figures 8 and 9 display similar qualitative profiles than Figures 2a and 2b. Roughly, similar conclusions can be obtained from the analysis of Fig. 9, being the smallest differences due to IL-XO_2 interactions.

LRC functionals provided an adequate description on the cation-anion interactions with energy deviations in the low limit. For IL-CO_2 systems, RMSD obtained by using LC-PBEPBE / CAM-B3LYP / ωB97X functionals in combination with 6-31+G** basis set are 0.51 Kcal mol^{-1}/ 0.56 Kcal mol^{-1}/ 0.66 Kcal mol^{-1}. These lower values in comparison with other standard functionals such as B3LYP, hybrid meta-GGA or dispersion corrected functionals could be attributed to a better charge transfer description. HF contribution in hybrid functionals (PBE0 and B3LYP) leads to smaller energy deviations. This effect is due to a better description of anion - XO_2 interactions using functionals with some HF contribution such as PBE0 and B3LYP, Fig. 6. The increasing % HF in hybrid meta-GGA functionals (from 27% up to 100%) leads to RMSD in the 0.68 Kcal mol^{-1} to 0.97 Kcal mol^{-1} range (using 6-31+G** basis set for IL-CO_2 systems). The inclusion of D2 approach on PBE and B3LYP functionals has similar effect than those previously noted for cation-anion interactions. For example at B3LYP/6-31+G* for IL-CO_2 systems, RMSD = 0.78 Kcal mol^{-1}, whereas RMSD = 0.94 Kcal mol^{-1} at B3LYP-D2/6-31+G* level. ωB97XD yields similar values than its partner without D2 approach (ωB97X). For ωB97XD/6-31+G* level, RMSD are 0.63 Kcal mol^{-1} / 1.05 Kcal mol^{-1} whereas RMSD = 0.65 Kcal mol^{-1} / 1.09 Kcal mol^{-1} at ωB97X/6-31+G* theoretical level, for CO_2 / SO_2 capture.

Regarding to binding energies estimated according with eq. 3 (Figures 10 and 11), they allow the analysis of IL-gas interactions. The effects of HF contribution in PBE0 and B3LYP functional (in comparison with pure PBE and BLYP functionals) as well as hybrid meta-GGA functionals upon increasing HF contributions are similar to those previously described for

anion-gas interactions. For IL-SO_2 systems in combination with 6-31+G** basis set, LC-PBEPBE / CAM-B3LYP yield RMSD = 0.79 Kcal mol^{-1} / 0.96 Kcal mol^{-1}, which are larger than RMSD values (0.77 Kcal mol^{-1} / 0.48 Kcal mol^{-1}) for their parent functionals without long range correction. Surprisingly, dispersion corrections (PBE-D2 /B3LYP-D2) leads to RMSD = 1.07 Kcal mol^{-1} / 1.06 Kcal mol^{-1}. As concerns to ωB97X and ωB97XD, RMSD = 0.88 1.07 Kcal mol^{-1} and 0.85 Kcal mol^{-1} are obtained. Therefore, long range and dispersion corrections have different effect on energy deviation depending on the scheme of selected functional.

Fig. 12 displays RMSD values of $\Delta E_{IL\text{-}XO2}$ taking into account both IL-CO_2 and IL-SO_2 families. The profile of Fig. 12 is very similar to those reported in Figures 6 and 7, which agrees with the fact that anion-XO_2 interactions play the main role in acid gas capture. The combination of both long range (allowing an adequate treatment of charge transfer processes) and dispersion corrections (suitable for describing weak interactions such as hydrogen bonding) in ωB97XD functionals seems a good choice for describing acid gas capture by ionic liquids at the molecular level. This study is focused on systems in which only cation-anion and ion-gas interactions are analyzed. Nonetheless, other interactions such as alkyl-alkyl side chain interactions or π-π stacking between aromatic ions could be also present in the IL bulk. Hence, dispersion corrections should be also considered for a proper treatment of such interactions.

Results reported in Figures 11 and 12 show that 6-31+G** and 6-311+G** basis sets provided higher energy deviations than 6-31G* basis set. Likewise, the effects of the selected functionals on optimized geometries also play an important role (Fig. 13). There are not remarkable changes in the relative arrangement between ion upon XO_2 presence, only the main IL-XO_2 distances were considered against the sum of van der Waals radii [61] as reference values. 6-31G* and aug-cc-PVDZ basis sets led to larger RMSD than 6-31+G** or 6-311+G** basis sets. PBE/6-31+G** theoretical level led to RMSD = 0.035 Å / 0.106 Å for IL-CO_2/SO_2 optimized geometries. Dispersion corrections (PBE-D2) led to RMSD = 0.043 Å / 0.111 Å for IL-CO_2/SO_2. Long range corrections (LC-PBEPBE) also yields larger deviations (RMSD = 0.053 Å / 0.123 Å for IL-CO_2/SO_2). Those effects were also inferred for B3LYP functional with RMSD = 0.036 Å / 0.108 Å, whereas CAM-B3LYP and B3LYP-D2 yielded RMSD = 0.044 Å / 0.108 Å and 0.039 Å / 0.107 Å, for IL-CO_2/SO_2. Likewise, ωB97X and ωB97XD functionals shown RMSD = 0.044 Å / 0.108 Å and 0.039 Å / 0.106 Å for IL-CO_2/SO_2. Most of measured IL-XO_2 distances are anion-XO_2 related with a charge transfer

interaction. Hence, conclusions here obtained are somewhat similar than those ones derived from cation-anion interactions.

3.4. CO_2/SO_2 Capture by ILs. The next objective in this work was to find suitable relationships between cation-anion, anion-XO_2 interactions and IL-XO_2 binding energies, which would allow to analyze the ability of selected ILs for acid gases capture purposes.

Results in previous sections shown three key factors for the study of IL-XO_2 systems: *i*) cation-anion interactions (which are the greatest contribution); *ii*) cation-XO_2 interactions; *iii*) anion-XO_2 interactions (which play a main role in the acid gas capture). Therefore, the development of mathematical relationships between the most relevant parameters characterizing these factors and gas capture efficiency is of great relevance. The simplest correlation would link $\Delta E_{IL\text{-}XO2}$ with cation-XO_2 and anion-XO_2 binding energies:

$$\Delta E_{IL\text{-}XO2} = a\Delta E_{cat\text{-}XO2} + b\Delta E_{ani\text{-}XO2} \quad (4)$$

where *a* and *b* are adjustable parameters giving account of the contribution from each ion. This equation would be able to predict gas capture efficiency through the optimization of only cation-XO_2 and anion-XO_2 systems. However, cation-anion interactions are the strongest forces even in the presence of gas molecules. $\Delta E_{IL\text{-}XO2}$ can be expressed as: $\Delta E_{IL\text{-}XO2} = \Delta E_{cat\text{-}ani\text{-}XO2} - c\Delta E_{IL}$. This assumption is only valid when the cation-anion binding energy is barely affected upon gas presence, and thus, *c* (which is also an adjustable parameter) should be $\simeq 1$. Eq. 4 can be rewritten as follows:

$$\Delta E_{cat\text{-}ani\text{-}XO2} = a\Delta E_{cat\text{-}XO2} + b\Delta E_{ani\text{-}XO2} + c\Delta E_{IL} \quad (5)$$

Parameters *a*, *b* and *c* were estimated through statistical fits at each theoretical level, Tables 2 (CO_2) and 3 (SO_2). RMSD and R^2 values (between $\Delta E_{cat\text{-}ani\text{-}XO2}$ estimated through Eq. 4 against binding energies from quantum chemistry calculations at the same level) have been also collected. Most methods yield parameters $a \simeq 0$, and $c \simeq 1$, while *b* is much larger than *a*. These results are in agreement with conclusions from previous sections, *i.e.* cation-anion interactions are not importantly affected by gas molecule ($c \simeq 1$), and anion-XO_2 interactions are the main force in acid gas capture by ionic liquids ($a \simeq 0$). Following the aim of obtaining simple relationships, we repeat the statistical fit according to eq. 6:

$$\Delta E_{cat\text{-}ani\text{-}XO2} = b\Delta E_{ani\text{-}XO2} + \Delta E_{IL} \quad (6)$$

where it is assumed that the interaction between both ions is not affected in presence of CO_2/SO_2 molecule (c=1), and anion-XO_2 interactions are the main parameter related with gas capture efficiency at the molecular level (a=0). Eq. 6 allows estimating $\Delta E_{cat\text{-}ani\text{-}XO2}$ only through the optimization of anion-XO_2 and cation-anion systems, which is useful for the rational design of ILs for acid gases capture, Tables 2 and 3. On average, selected methods

led to RMSD = 0.25 Kcal mol^{-1} / 0.71 Kcal mol^{-1} and R^2= 0.9596 / 0.7734 for CO_2 / SO_2 capture, which could be considered as reasonable values because of the diversity in the chemical structure of selected ILs (e. g. $\Delta E_{cat\text{-}ani\text{-}XO2}$ are ranged between 80 and 130 Kcal mol^{-1}). In spite of the pivotal role of anions for acid gas capture, the quality of the reported fits is lower for SO_2 than for CO_2 capture, which points out to factors such as cation-gas interactions or weakening of cation-anion interactions also influencing acid gases capture. Therefore, simple relationship (as those defined by Eq. 6) could be very useful in the rational design of task specific ionic liquids for acid gas capture. For example, the general trends for big families of ILs could be analyzed only based on the study of anion-XO_2 and anion-cation systems, avoiding the study of IL-XO_2 systems (which would need the largest computational effort).

The analysis of parameter *b* estimated at each theoretical revel could be also used for the assessment of DFT methods and of the trends followed by the studied ILs. At MP2/aug-cc-pvDZ reference level, *b* = 0.87 / 0.77 for CO_2/SO_2 capture. In combination with 6-31+G** basis set (although similar conclusions may be inferred for any basis set). PBE and BLYP functional pure functionals provide *b* = 0.18 / 0.75 and 0.24 / 0.50, while *b* = 0.66 / 0.74 and 0.63 / 0.72 for hybrid functionals (PBE0 and B3LYP) for CO_2/SO_2. For hybrid meta-GGA functionals, *b* lies between 0.83 and 1.11 / 0.94 and 0.96 for CO_2/SO_2. In general, the presence of HF contribution leads to growing *b* values, which is related with increasing contribution from $\Delta E_{ani\text{-}XO2}$ to the total $\Delta E_{cat\text{-}ani\text{-}XO2}$ energy values. Similar conclusions are obtained for LC-PBEPBE (*b* = 1.02 / 1.01), CAM-B3LYP (*b* = 0.90 / 0.94) and ωB97X (*b* = 0.93 / 0.90) functionals. Dispersion corrected functionals also led to $b \simeq 1.0$. In short, high HF contribution, long range corrections as well as D2 approach brings larger *b* values than MP2 reference level. Despite the variation in *b* values, all selected methods yields acceptable fit results according to eq. 6. Therefore, any of the studied DFT methods in this work could be used to study the trends between different ionic liquids. As example, Fig. 14 displays ΔE_{IL} and $\Delta E_{IL\text{-}XO2}$ values estimated for each selected method in combination with aug-cc-pvDZ basis set (similar qualitative profiles are obtained for Pople's basis sets). In general, BLYP and HF methods provide the lowest binding energy values, although BLYP/aug-cc-pvDZ led to some negative $\Delta E_{IL\text{-}XO2}$ values. The largest difference between selected DFT methods and MP2 reference level are noted for $\Delta E_{IL\text{-}SO2}$ values, concretely for IL 40-54 (which are based on imidazol cation paired with $[SCN]^-$, $[DCA]^-$ or halides anions). Nonetheless, the studied DFT methods yielded the same profile with low RMSD values for the whole set of ILs (Fig. 11).

HF method provides the largest deviations from reference level both in energy values and patterns.

ωB97XD functional fulfils two basic requisites for an adequate treatment of acid gases capture by ILs at the molecular level: *i*) long range corrections, providing suitable charge transfer description (from the anion to the cation or from the anion to the XO_2 molecule), and *ii*) the use of dispersion corrections, which also brings an improvement on the description of ion-XO_2 interactions. Moreover, dispersion corrections also provide a proper treatment of other relevant interactions for certain types of ions such as alkyl-alkyl side chain interactions or π-π stacking between aromatic ions. This functional was also able to provide low RMSD values for modest basis set such as 6-31+G**.

The suitability of the studied ILs for acid gas capture is analyzed using ωB97XD/6-31+G** level (Fig. 15). The comparison of calculated binding energy values with experimental data was done using IL 22 ([EMIM][NTf_2]), which was selected because of its CO_2 capture performance demonstrated experimentally.[14] IL 22 yields ΔE_{IL} = 79.04 Kcal mol^{-1}, while $\Delta E_{cat\text{-}ani\text{-}CO2}$ = 81.08 Kcal mol^{-1} and $\Delta E_{IL\text{-}CO2}$ = 2.04 Kcal mol^{-1}. This energy could be considered as a low limit, from which higher values would be adequate to provide high gas affinities. Based on our results, most of the ILs studied in this work could be considered as candidates for acid gases capturing purposes with improved efficiencies. ILs 14 ([EMIM][Et_2PO_4]), 19 ([EMIM][Ac]), 34 ([B4MPy][NTf_2]), 37 ([HMIM][SO_3CF_3]), 41 ([EMIM][DCA]) and 46 ([EMIM][Cl]) yielded high binding energies for both CO_2 and SO_2 gases, and thus, they could be used for the simultaneous capture of both acid gases. Further studies should be adequate to elucidate the most suitable ion combinations for obtaining high binging energies. Nevertheless, the suitability of any IL for capturing acid gas with technological applications also depends on other properties related with the macroscopic fluids' behavior such as melting point, density, viscosity or diffusion coefficients as well as the effect of absorbed gases on these properties, which is far from the aim of this paper. Nevertheless, the selection of ILs with high gas affinities through DFT could be the first step in the rational design of IL for acid gases capture purposes.

4. CONCLUSIONS

In this paper, we assess the performance of a range set of several density functional methods to study binding energies related with acid gas capture (CO_2 and SO_2) by ionic liquids (ILs). Different approximations such as pure GGA (PBE and BLYP), hybrid meta-GGA (M06, M06-2X and M06-HF), long range corrected (LC-PBEPBE, CAM-B3LYP, ωB97X) and dispersion corrected (PBE-D2, B3LYP-D2 and ωB97XD) functionals, as well as

HF and MP2 methods were also applied. Thus, the performance of 15 different methods in combination with four basis sets (6-31G*, 6-31+G**, 6-311+G** and aug-cc-pvDZ) was evaluated based on MP2/aug-cc-pvDZ reference values for a set of 54 ILs. There are key factors in the study of gas acid capture by ILs at the molecular level: *i*) cation-anion interactions (which are the greatest contribution); *ii*) cation-XO_2 interactions; *iii*) anion-XO_2 interactions. Hence, binding energies of cation-anion interacting pairs as well as IL-CO_2 and IL-SO_2 systems were calculated. Our simulations have shown that an appropriate description of charge transfer process (from the anion to the cation and from the anion to gas molecule as well) are adequate for the study of cation-anion and anion-gas interactions. Thus, ωB97X ωB97XD functionals provide RMSD in the low range in comparison with other stand functionals. Even though, any of the studied DFT methods in this work could be used to study the qualitative trends between different ionic liquids. In our opinion, although ωB97XD did not yield the lowest deviation, this functional fulfils two basic requisites for an adequate treatment of acid gases capture by ILs at the molecular level: *i*) long range corrections, providing suitable charge transfer description, and *ii*) the use of dispersion corrections, which also brings an improvement on the description of ion-XO_2 interactions. This functional was also able to provide low RMSD values for modest basis set such as 6-31+G**. In addition, dispersion corrections are also adequate for a proper treatment of other relevant interactions for certain types of ions such as alkyl-alkyl side chain interactions or π-π stacking between aromatic ions, which play an important role in the IL bulk.

Finally, useful relationships between cation-anion, anion-XO_2 interactions and IL-XO_2 binding energies were also developed. The obtained correlations show the pivotal role of anion-XO_2 interactions in the acid gas capture by ionic liquids. Thus, based on the simplest relationship, the gas capture efficiency could be study gas only through the optimization of only cation-anion and anion-XO_2 systems. This is a useful result for the rational design of ILs for acid gases capture through screening process avoiding the optimization of cation- XO_2 and IL- XO_2 systems.

ACKNOWLEDGEMENTS

This work was made possible by Ministerio de Economía y Competitividad (Spain, project CTQ2013-40476-R) and Junta de Castilla y León (Spain, project BU324U14). Gregorio García acknowledges the funding by Junta de Castilla y León, cofunded by European Social Fund, for a postdoctoral contract. We also acknowledge The Foundation of Supercomputing Center of Castile and León (FCSCL, Spain), Computing and Advanced Technologies

Foundation of Extremadura (CénitS, LUSITANIA Supercomputer, Spain), and Consortium of Scientific and Academic Services of Cataluña (CSUC, Spain) for providing supercomputing facilities. The statements made herein are solely the responsibility of the authors.

REFERENCES

1. N. V. Plechkova, K. R. Seddon, *Chem. Soc. Rev.,* 2008**, 37**, 123-150; S. Tang, G. A. Baker, H. Zhao, *Chem. Soc. Rev.,* 2012**, 41**, 4030-4066; S. Aparicio, M. Atilhan, F. Karadas, *Ind. Eng. Chem. Res.,* 2010**, 49**, 9580-9595.
2. F. Karadas, M. Atilhan, S. *Energy & Fuels,* 2010**, 24**, 5817-5828.
3. R. Ren, Y. Hou, S. Tian, X. Chen, W. Wu, *J. Phys. Chem. B, 2013***, 117**, 2482-2486; Z. Lei, C. Dai, B. Chen, *Chem. Rev.,*2014, **114**, 1289-1326.
4. A. A. Lacis, G. A. Schmidt, D. Rind, R. A. Ruedy, *Science* 2010, **330**, 356-359; S. J. Smith, J. van Aardenne, Z. Klimont, R. J. Andres, A. Volke, S. Delgado Arias, *Atmos. Chem. Phys.* 2011, **11**, 1101-1116; G. Cui, C.Wang, J. Zheng, Y.Guo, X. Luo, H. Li, *Chem. Comm.,* 2012, **48**, 2633-2635
5. J. Huang, A. Riisager, P. Wasserscheid, R. Fehrmann, *Chem. Comm.,* 2006**,** 4027-4029.
6. G. T. Rochelle, *Science* 2009, **325**, 1652-1654.
7. L. Raynal, P. A. Bouillon, A. Gomez, P. Broutin, *Chemical Engineering Journal,* 2011, **171**, 742-752.
8. A. J. Sexton, G. T. Rochelle, *Ind. Eng. Chem. Res.,* 2010, **50**, 667-673.
9. J. Kittel, R. Idem, D. Gelowitz, P. Tontiwachwuthikul, G. Parrain, A. Bonneau, *Energy Procedia,* **2009, 1**, 791-797.
10. L. M. Romeo, I. Bolea, J. M. Escosa, *Applied Thermal Engineering* 2008, ***28***, 1039-1046.
11. J. Husebye, A. L. Brunsvold, S. Roussanaly, X. Zhang, *Energy Procedia* 2012, **23**, 381-390.
12. A. Maiti, *J. Quantum Chem.,* 2014, **114**, 163-175; S. Aparicio, M. Atilhan, *Chemical Physics,* 2012, **400**, 118-125; H. Liu, S. Dai, D.E. Jiang, *J. Phys. Chem. B,* 2014, **118**, 2719-2725; S. Aparicio, M. Atilhan, *Energy & Fuels, 2013,* **27**, 2515-2527; S. Aparicio, M. Atilhan, *J. Chem. Phys. B* **2012,** *116*, 9171-9185; S. Aparicio, M. Atilhan, *Energy & Fuels,* 2010, **24**, 4989-5001; J. D. Morganti, K. Hoher, M. C. C. Ribeiro, R. A. Ando, L. J. A. Siqueira, *J. Phys. Chem. C,*2014**, 118**, 22012-22020; M. Mohammadi, M. Foroutan, *Journal of Molecular Liquids,* 2014*,* **193**, 60-68; D. Firaha, M. Kavalchuk, B. Kirchner, *J. Solution. Chem.,* 2015, **44**, 838-849. B. Kirchner, O. Hollóczki, J. N. Canongia Lopes, A. A. H. Pádua, *WIREs Comput. Mol. Sci.,* 2015**, 5**, 202-214; C. Cadena, J. L. Anthony, J. K. Shah, T. I. Morrow, J. F. Brennecke, E. J. Maginn, *J. Am. Chem. Soc.*, 2004**, 126**, 5300-5308; W. Shi, E. J. Maginn, *J. Phys. Chem. B,* 2008**, 112**, 2045-2055; E. J. Maginn, *J. Phys.: Condens. Matter,* 2009**, 21**, 373101/1-373101/17.
13. S. Aparicio, M. Atilhan, M. Khraisheh, R. Alcalde, J. Fernández, *J. Phys. Chem. B,* 2011, **115**, 12487-12498; C. Wu, T. P. Senftle, W. F.Schneider, *Phys. Chem. Chem. Phys.,* 2012, **14**, 13163-13170. ; K. M. Gupta, J. Jiang, *J. Phys. Chem. C,* **2014,** *118*, 3110-3118; B. Gurkan, B. F. Goodrich, E. M. Mindrup, L. E. Ficke, M. Massel, S. Seo, T. P. Senftle, H. Wu, M. F. Glaser, J. K. Shah, E. J. Maginn, J. F. Brennecke, W. F. Schneider, *J. Phys. Chem. Lett.,* 2010**, 1**, 3494-3499.
14. F. Karadas, B. Köz, J. Jacquemin, E. Deniz, D. Rooney, J. Thompson, C. T. Yavuz, M. Khraisheh, S. Aparicio, M. Atihan, *Fluid Phase Equilibria, 2013,* **351**, 74-86.
15. O. Hollóczki, Z. Kelemen, L. Könczöl, D. Szieberth, L. Nyulászi, A. Stark, B. Kirchner, *ChemPhysChem,* 2013, **14**, 315-320; V. Sanz, R. Alcalde, M. Atilhan, S. Aparicio, *J. Mol. Model.,* 2014, **20**, 1-14; F. Yan, M. Lartey, K. Damodaran, E. Albenze, R. L. Thompson, J. Kim, M. Haranczyk, H. B. Nulwala, D. R. Luebke, B. Smit, *Phys. Chem. Chem. Phys.,* 2013, **15**, 3264-3272;
16. G. B. Damas, A. B. A. Dias, L. T. Costa, *J. Phys. Chem. B,* 2014, **118**, 9046-9064.
17. P. Gu, R. Lü, S. Wang, Y. Lu, D. Liu, *Computational and Theoretical Chemistry.* 2013**, 1020**, 22-31; G. Yu, X. Chen, *J. Phys. Chem. B,* 2011**, *115***, 3466-3477.
18. C. Lee, W. Yang, R. G. Parr, *Phys. Rev. B,* 1988, **37**, 785-789.
19. A. D Becke, *J. Chem. Phys.,* 1993, **98**, 5648.
20. A. D. Becke, *Phys. Rev. A,* 1988**, 38**, 3098-3100.
21. A. J. Cohen, P. Mori-Sánchez, W. Yang, *Chem. Rev.,*2012, **112,** 289-320.
22. S. N. Steinmann, C. Piemontesi, A. Delachat, C. Corminboeuf, *J. Chem. Theory Comput.,* 2012, **8**, 1629-1640.
23. J. Rigby, E. I. Izgorodina, *J. Chem. Theory Comput.,* 2014, **10**, 3111-3122.
24. E. I. Izgorodina, U. L. Bernard, D. R. MacFarlane, *J. Phys. Chem. A,* 2009, **113**, 7064-7072.
25. S. Zahn, D. R. MacFarlane, E. I. Izgorodina, *Phys. Chem. Chem. Phys.,* 2013, **15**, 13664-13675.
26. S. Zahn, B. Kirchner, *J. Phys. Chem. A,* 2008, **112**, 8430-8435.
27. S. Grimme, W. Hujo, B Kirchner, *Phys. Chem. Chem. Phys.,* 2012, **14**, 4875-4883.

28. R. A. Ando, L. J. A. Siqueira, F. C. Bazito, R. M. Torresi, P. S. Santos, *J. Phys. Chem. B,* 2007**, 111**, 8717-8719; L. J. A. Siqueira, R. A. Ando, F. F. C. Bazito, R. M. Torresi, P. S. Santos, M. C. C. Ribeiro, *J. Phys. Chem. B,* 2008, **112**, 6430-6435.
29. C. Moller, M. S. Plesset, *Phys. Rev* **1934,** *46*, 618-622; M. Head-Gordon, J. A. Pople, M. J. Frisch, *Chemical Physics Letters,* 1988, **153**, 503-506.
30. G.Garcia,; M. Atilhan, S. Aparicio, *Phys. Chem. Chem. Phys.,* 2015, **17**, 13559-13574.
31. M. J. Frisch, G. W. Trucks, H. B. Schlegel, G. E. Scuseria, M. A. Robb, J. R. Cheeseman, G. Scalmani, V. Barone, B. Mennucci, G. A. Petersson, H. Nakatsuji, M. Caricato, X. Li, H. P. Hratchian, A. F. Izmaylov, J. Bloino, G. Zheng, J. L. Sonnenberg, M. Hada, M. Ehara, K. Toyota, R. Fukuda, J. Hasegawa, M. Ishida, T. Nakajima, Y. Honda, O. Kitao, H. Nakai, T. Vreven, J. A. Montgomery, Jr., J. E. Peralta, F. Ogliaro, M. Bearpark, J. J. Heyd, E. Brothers, K. N. Kudin, V. N. Staroverov, R. Kobayashi, J. Normand, K. Raghavachari, A. Rendell, J. C. Burant, S. S. Iyengar, J. Tomasi, M. Cossi, N. Rega, J. M. Millam, M. Klene, J. E. Knox, J. B. Cross, V. Bakken, C. Adamo, J. Jaramillo, R. Gomperts, R. E. Stratmann, O. Yazyev, A. J. Austin, R. Cammi, C. Pomelli, J. W. Ochterski, R. L. Martin, K. Morokuma, V. G. Zakrzewski, G. A. Voth, P. Salvador, J. J. Dannenberg, S. Dapprich, A. D. Daniels, Ö. Farkas, J. B. Foresman, J. V. Ortiz, J. Cioslowski, and D. J. Fox, Gaussian 09, Revision **D.01**, Gaussian, Inc.: Wallingford, CT, USA, 2009.
32. J. P. Perdew, K. B. Ernzerhof, *Phys. Rev. Lett.,* 1996**, 77**, 3865.
33. C. Adamo, V. Barone, *J. Chem. Phys.* 1999**, 110**, 6158-6170.
34. Y. Zhao, D. G. Truhlar, *Acc. Chem. Res.,* 2008, **41**, 157-167.
35. Y. Zhao, D. Truhlar, *Thero. Chem. Account., 2008,* **120**, 215-241.
36. Y. Zhao, D. G. Truhlar, *J. Phys. Chem. A,* 2006, **110**, 13126-13130.
37. D. V. Banthorpe, *Chem. Rev.,*1970, **70**, 295-322; J. Prissette, G. Seger, E. Kochanski, *J. Am. Chem. Soc.,* 1978, **100**, 6941-6947.
38. T. Bally, G. N. Sastry, *J. Phys. Chem. A,* 1997, **101,** 7923-7925; O. V. Gritsenko, B. Ensing, P. R. T. Schipper, E. J. Baerends, *J. Phys. Chem. A,* 2000, **104**, 8558-8565.
39. T. Tsuneda, K. Hirao, *WIREs comput. Mol. Sci.,* 2014, **4**, 375-390.
40. H. Iijura, T. Tsuneda, T. Yanai, K.Hirao, *J. Chem. Phys.* 2001, **115**, 3540-3544.
41. T. Yanai, D. P. Tew, N. C. Handy, *Chemical Physics Letters,* 2004, **393**, 51-57.
42. J. D. Chai, M. Head-Gordon, *J. Chem. Phys.,* 2008, **128**, 084106/1-084106/15.
43. S.Grimme, *J. Comput. Chem.,* 2006, **27**, 1787-1799.
44. J. D. Chai, M. Head-Gordon, *Phys. Chem. Chem. Phys.,* 2008, **10**, 6615-6620.
45. T. Schwabe, S. Grimme, *Phys. Chem. Chem. Phys.,* 2007, **9**, 3397-3406.
46. S. Grimme, J. Antony, S. Ehrlich, H. Krieg, *J. Chem. Phys.,* 2010**, 132**, 154104/1-154104/19.
47. S. Grimme, S. Ehrlich, L. Goerigk, *J. Comput. Chem.,* 2011, **32**, 1456-1465.
48. Y. S. Lin, G. D. Li, S.P. Mao, J. D. Chai, *J. Chem. Theory Comput.,* 2013, **9**, 263-272.
49. E. Brémond, C. Adamo, *J. Chem. Phys.,* 2011, **135**, 024106/1-024106/6.
50. S. Grimme, *J. Chem. Phys.* 2006, **124**, 034108/1-034108/16.
51. D. Bousquet, E. Brémond, J. C. Sancho-García, I. Ciofini, C. Adamo, *J. Chem. Theory Comput.,* 2013, **9**, 3444-3452.
52. T. Benighaus, R. A. DiStasio, R. C. Lochan, J. D. Chai, M. Head-Gordon, *J. Phys. Chem. A,* 2008, **112**, 2702-2712.
53. Y. Zhao, D. G. Truhlar, *J. Chem. Theory Comput.,* 2006, **3**, 289-300.
54. S. Tsuzuki, A. A. Arai, K. Nishikawa, *J. Phys. Chem. B,* 2008, **112**, 7739-7747; P. A. Hunt, I. R. Gould, *J. Phys. Chem. A,* 2006, **110**, 2269-2282; C. Fong-Padrón, E. M. Cabaleiro-Lago, J. Rodríguez-Otero, *Chemical Physics Letters,* 2014**, 593**, 181-188.
55. Y. Zhao, D. G.Truhlar, *J. Chem. Theory Comput.,* 2007, **3**, 289-300.
56. S. Tsuzuki, H. Tokuda, K. Hayamizu, M. Watanabe, *J. Phys. Chem. B,*2005, **109**, 16474-16481.
57. N. X. Wang, K. Venkatesh, A. K. Wilson, *J. Phys. Chem. A,* 2005, **110**, 779-784.
58. J. Marten, W. Seichter, E. Weber, U.Bohme, *CrystEngComm,* 2008, **10**, 541-547.
59. S. Simon, M. Duran, J. J. Dannenberg*J. Chem. Phys.,* 1996, **105**, 11024.
60. C. M. Breneman, K. B . Wiberg, *J. Comput. Chem.,* 1990, **11**, 361-373.
61. S. S. Batsanov, *Inorganic Materials,* 2001, **37**, 871-885.

Table 1. Selected family of ionic liquids studied in this work.

numbering	cation	anion	labeling
1	1-ethyl-3-methylimidazolium	tetrafluoroborate	[EMIM][BF_4]
2	1-butyl-3-methylimidazolium	tetrafluoroborate	[BMIM][BF_4]
3	1-hexyl-3-methylimidazolium	tetrafluoroborate	[HMIM][BF_4]
4	1-methyl-3-octylimidazolium	tetrafluoroborate	[OMIM][BF_4]
5	1-butylpyridinium	tetrafluoroborate	[BPy][BF_4]
6	1-butyl-3-methylpyridinium	tetrafluoroborate	[B3MPy][BF_4]
7	1-butyl-4-methylpyridinium	tetrafluoroborate	[B4MPy][BF_4]
8	1-butyl-3-methylimidazolium	hexafluorophosphate	[BMIM][PF_6]
9	1-hexyl-3-methylimidazolium	hexafluorophosphate	[HMIM][PF_6]
10	1-methyl-3-octylimidazolium	hexafluorophosphate	[OMIM][PF_6]
11	1-butylpyridinium	hexafluorophosphate	[BPy] [PF_6]
12	1-butyl-3-methylpyridinium	hexafluorophosphate	[B3MPy][PF_6]
13	1-butyl-4-methylpyridinium	hexafluorophosphate	[B4MPy][PF_6]
14	1-ethyl-3-methylimidazolium	diethylphosphate	[EMIM][Et_2PO_4]
15	1,3-dimethylimidazolium	dimethylphosphate	[DMIM][Me_2PO_4]
16	choline	dihydrogenphosphate	[CH][H_2PO_4]
17	1-ethyl-3-methylimidazolium	ethylsulfate	[EMIM][$EtSO_4$]
18	1-ethyl-3-methylimidazolium	hidrogensulfate	[EMIM][HSO_4]
19	1-ethyl-3-methylimidazolium	acetate	[EMIM][Ac]
20	ethylammonium	nitrate	[$EtNH_3$][NO_3]
21	triethylsulfonium	bis[(trifluoromethyl)sulfonyl]imide	[Et_3S][NTf_2]
22	1-ethyl-3-methylimidazolium	bis[(trifluoromethyl)sulfonyl]imide	[EMIM][NTf_2]
23	1-methyl-3-propylimidazolium	bis[(trifluoromethyl)sulfonyl]imide	[MPIm][NTf_2]
24	1,2-dimethyl-3-propylimidazolium	bis[(trifluoromethyl)sulfonyl]imide	[DMPIm][NTf_2]
25	1-butyl-3-methylimidazolium	bis[(trifluoromethyl)sulfonyl]imide	[BMIM][NTf_2]
26	1-butyl-2,3-dimethylimidazolium	bis[(trifluoromethyl)sulfonyl]imide	[BDMIM][NTf_2]
27	1-hexyl-3-methylimidazolium	bis[(trifluoromethyl)sulfonyl]imide	[HMIM][NTf_2]
28	1-allyl-3-methylimidazolium	bis[(trifluoromethyl)sulfonyl]imide	[AMIM][NTf_2]
29	1-methyl-1-propylpyrrolidinium	bis[(trifluoromethyl)sulfonyl]imide	[MPPyr][NTf_2]
30	1-butyl-1-methylpyrrolidinium	bis[(trifluoromethyl)sulfonyl]imide	[BMPyr][NTf_2]
31	1-methyl-1-propylpiperidinium	bis[(trifluoromethyl)sulfonyl]imide	[MPPipe][NTf_2]
32	1-butylpyridinium	bis[(trifluoromethyl)sulfonyl]imide	[BPy][NTf_2]
33	1-butyl-3-methylpyridinium	bis[(trifluoromethyl)sulfonyl]imide	[B3MPy][NTf_2]
34	1-butyl-4-methylpyridinium	bis[(trifluoromethyl)sulfonyl]imide	[B4MPy][NTf_2]
35	1-ethyl-3-methylimidazolium	triflate	[EMIM][SO_3CF_3]
36	1-butyl-3-methylimidazolium	triflate	[BMIM][SO_3CF_3]
37	1-hexyl-3-methylimidazolium	triflate	[HMIM][SO_3CF_3]
38	1-methyl-3-octhylimidazolium	triflate	[OMIM][SO_3CF_3]
39	1-butyl-1-methylpyrrolidinium	triflate	[BMPyr][SO_3CF_3]
40	1-ethyl-3-methylimidazolium	thiocianate	[EMIM][SCN]
41	1-ethyl-3-methylimidazolium	dicyanamide	[EMIM][DCA]
42	1-butyl-3-methylimidazolium	dicyanamide	[BMIM][DCA]
43	1-butyl-1-methylpyrrolidinium	dicyanamide	[BMPyr][DCA]
44	1-ethyl-3-methylimidazolium	chloride	[EMIM][Cl]
45	1-butyl-3-methylimidazolium	chloride	[BMIM][Cl]
46	1-allyl-3-methylimidazolium	chloride	[AMIM][Cl]
47	1-ethyl-3-methylimidazolium	bromide	[EMIM][Br]
48	1-butyl-3-methylimidazolium	bromide	[BMIM][Br]
49	1,3-dimethylimidazolium	iodide	[DMIM][I]
50	1-ethyl-3-methylimidazolium	iodide	[EMIM][I]
51	1-methyl-3-propylimidazolium	iodide	[MPIm][I]
52	1-butyl-3-methylimidazolium	iodide	[BMIM][I]
53	1-hexyl-3-methylimidazolium	iodide	[HMIM][I]
54	1-allyl-3-methylimidazolium	iodide	[AMIM][I]

Table 2. Results from the fit of $\Delta E_{cat\text{-}ani\text{-}CO2}$ according to eqs. 5 and 6.

		$\Delta E_{cat\text{-}ani\text{-}CO2} = a\Delta E_{cat\text{-}CO2} + b\Delta E_{ani\text{-}CO2} + c\Delta E_{IL}$					$\Delta E_{cat\text{-}ani\text{-}CO2} = b\Delta E_{ani\text{-}CO2} + \Delta E_{IL}$		
					RMSD /			RMSD /	
		a	*b*	*c*	Kcal mol^{-1}	R^2	*b*	Kcal mol^{-1}	R^2
PBE	6-31G*	$1.30\cdot10^{-9}$	0.11	1.01	0.15	0.9886	0.31	0.19	0.9821
	6-31+G**	$5.04\cdot10^{-9}$	0.22	1.02	0.16	0.9852	0.57	0.18	0.9823
	6-311+G**	$4.95\cdot10^{-9}$	0.30	1.04	0.13	0.9911	0.60	0.22	0.9745
	aug-cc-pvDZ	$3.87\cdot10^{-10}$	$6.73\cdot10^{-9}$	1.03	0.13	0.9921	0.39	0.17	0.9861
BLYP	6-31G*	$4.79\cdot10^{-10}$	0.17	1.00	0.16	0.9870	0.20	0.17	0.9868
	6-31+G**	$9.05\cdot10^{-9}$	0.04	1.02	0.18	0.9811	0.34	0.24	0.9677
	6-311+G**	$3.20\cdot10^{-9}$	0.13	1.02	0.12	0.9920	0.53	0.14	0.9885
	aug-cc-pvDZ	$1.30\cdot10^{-9}$	$2.33\cdot10^{-9}$	1.04	0.15	0.9889	0.73	0.26	0.9677
PBE0	6-31G*	$3.70\cdot10^{-9}$	0.15	1.02	0.16	0.9869	0.44	0.21	0.9754
	6-31+G**	$4.42\cdot10^{-9}$	0.20	1.03	0.15	0.9873	0.66	0.17	0.9829
	6-311+G**	$7.95\cdot10^{-9}$	0.09	1.04	0.13	0.9896	0.70	0.22	0.9719
	aug-cc-pvDZ	$4.54\cdot10^{-9}$	0.02	1.03	0.14	0.9903	0.54	0.17	0.9863
B3LYP	6-31G*	$3.53\cdot10^{-9}$	0.15	1.01	0.16	0.9876	0.42	0.19	0.9823
	6-31+G**	$4.12\cdot10^{-9}$	0.68	0.99	0.14	0.9887	0.63	0.14	0.9887
	6-311+G**	$4.06\cdot10^{-9}$	0.53	1.01	0.12	0.9913	0.64	0.12	0.9912
	aug-cc-pvDZ	$1.85\cdot10^{-9}$	1.14	0.96	0.21	0.9795	1.13	0.23	0.9748
M06	6-31G*	$4.51\cdot10^{-9}$	0.73	1.00	0.23	0.9699	0.80	0.23	0.9667
	6-31+G**	$5.62\cdot10^{-9}$	1.02	0.99	0.22	0.9670	0.92	0.22	0.9669
	6-311+G**	$9.55\cdot10^{-9}$	0.21	1.05	0.22	0.9664	0.88	0.23	0.9621
	aug-cc-pvDZ	$0.99\cdot10^{-9}$	1.52	0.92	0.22	0.9704	0.89	0.25	0.9626
M06-2X	6-31G*	$7.19\cdot10^{-10}$	0.55	1.02	0.30	0.9453	0.79	0.30	0.9430
	6-31+G**	$1.11\cdot10^{-8}$	0.82	1.02	0.23	0.9615	1.11	0.24	0.9602
	6-311+G**	$1.10\cdot10^{-8}$	0.49	1.03	0.23	0.9618	0.90	0.23	0.9591
	aug-cc-pvDZ	$2.07\cdot10^{-7}$	0.51	1.02	0.21	0.9726	0.82	0.21	0.9718
M06-HF	6-31G*	$7.00\cdot10^{-9}$	0.25	1.04	0.32	0.9429	0.64	0.37	0.9258
	6-31+G**	$1.85\cdot10^{-8}$	0.39	1.04	0.26	0.9602	0.83	0.28	0.9536
	6-311+G**	$1.00\cdot10^{-8}$	0.29	1.05	0.25	0.9586	0.82	0.30	0.9410
	aug-cc-pvDZ	$0.05\cdot10^{-2}$	0.01	1.05	0.23	0.9850	0.25	0.54	0.9193
LC-PBEPB	6-31G*	$3.31\cdot10^{-9}$	0.33	1.03	0.28	0.9572	0.77	0.31	0.9483
	6-31+G**	$8.32\cdot10^{-9}$	0.81	1.03	0.24	0.9642	1.02	0.24	0.9635
	6-311+G**	$4.44\cdot10^{-9}$	0.12	1.06	0.24	0.9610	1.00	0.28	0.9475
	aug-cc-pvDZ	$1.92\cdot10^{-9}$	0.04	1.05	0.24	0.9686	0.91	0.28	0.9577
CAM-B3LYP	6-31G*	$3.90\cdot10^{-9}$	0.23	1.03	0.30	0.9552	0.58	0.35	0.9381
	6-31+G**	$7.01\cdot10^{-9}$	0.35	1.04	0.27	0.9592	0.90	0.30	0.9489
	6-311+G**	0.11	0.12	1.05	0.26	0.9596	0.93	0.34	0.9323
	aug-cc-pvDZ	$1.46\cdot10^{-9}$	0.04	1.04	0.23	0.9738	0.72	0.28	0.9591
ωB97X	6-31G*	$1.48\cdot10^{-9}$	0.44	1.02	0.25	0.9610	0.75	0.26	0.9583
	6-31+G**	$7.68\cdot10^{-9}$	0.55	1.03	0.20	0.9705	0.93	0.21	0.9687
	6-311+G**	$4.66\cdot10^{-9}$	0.30	1.05	0.20	0.9687	0.92	0.21	0.9664
	aug-cc-pvDZ	$1.96\cdot10^{-10}$	0.15	1.04	0.18	0.9803	0.80	0.20	0.9769
PBE-D2	6-31G*	$1.06\cdot10^{-9}$	0.22	1.03	0.21	0.9696	0.62	0.24	0.9617
	6-31+G**	$3.96\cdot10^{-9}$	0.21	1.07	0.26	0.9484	1.05	0.35	0.9064
	6-311+G**	$2.53\cdot10^{-9}$	0.04	1.06	0.19	0.9723	0.89	0.22	0.9621
	aug-cc-pvDZ	0.77	0.77	0.98	0.25	0.9591	1.14	0.29	0.9449
B3LYP-D2	6-31G*	$1.05\cdot10^{-9}$	0.49	1.02	0.23	0.9587	0.84	0.24	0.9555
	6-31+G**	$6.77\cdot10^{-9}$	0.82	1.02	0.23	0.9526	1.04	0.24	0.9520
	6-311+G**	$1.06\cdot10^{-9}$	0.24	1.06	0.21	0.9558	1.06	0.23	0.9495
	aug-cc-pvDZ	$4.57\cdot10^{-13}$	0.35	1.06	0.21	0.9649	0.81	0.29	0.9360
ωB97XD	6-31G*	0.36	0.36	1.01	0.42	0.8829	0.83	0.44	0.8712
	6-31+G**	$1.52\cdot10^{-8}$	0.41	1.04	0.20	0.9686	1.05	0.22	0.9584
	6-311+G**	$1.22\cdot10^{-8}$	0.15	1.05	0.18	0.9707	1.02	0.23	0.9542
	aug-cc-pvDZ	$1.17\cdot10^{-9}$	0.09	1.04	0.17	0.9802	0.89	0.21	0.9682
HF	6-31G*	$8.96\cdot10^{-9}$	0.22	1.03	0.17	0.9819	0.69	0.20	0.9757
	6-31+G**	$1.23\cdot10^{-8}$	0.43	1.02	0.14	0.9854	0.79	0.15	0.9841
	6-311+G**	$1.31\cdot10^{-9}$	0.09	1.04	0.20	0.9742	0.84	0.21	0.9701
	aug-cc-pvDZ	0.18	0.18	1.02	0.20	0.9760	0.77	0.24	0.9654
MP2	6-31G*	$7.60\cdot10^{-9}$	0.17	1.03	0.20	0.9751	0.58	0.37	0.9180
	6-31+G**	$8.16\cdot10^{-9}$	0.43	1.03	0.23	0.9629	0.88	0.28	0.9459
	6-311+G**	$4.12\cdot10^{-11}$	$5.61\cdot10^{-10}$	1.05	0.16	0.9784	0.83	0.30	0.9275
	aug-cc-pvDZ	$2.07\cdot10^{-11}$	$0.06\cdot10^{-2}$	1.04	0.14	0.9859	0.87	0.17	0.9792

Table 3. Results from the fit of $\Delta E_{cat\text{-}ani\text{-}SO2}$ according to eqs. 5 and 6.

		$\Delta E_{cat\text{-}ani\text{-}SO2} = a\Delta E_{cat\text{-}SO2} + b\Delta E_{ani\text{-}SO2} + c\Delta E_{IL}$					$\Delta E_{cat\text{-}ani\text{-}SO2} = b\Delta E_{ani\text{-}SO2} + \Delta E_{IL}$		
		a	b	c	RMSD / Kcal mol^{-1}	R^2	b	RMSD / Kcal mol^{-1}	R^2
PBE	6-31G*	$1.23\cdot10^{-8}$	0.15	1.08	0.54	0.8969	0.67	0.62	0.8637
	6-31+G**	$1.65\cdot10^{-8}$	0.28	1.08	0.72	0.8318	0.75	0.77	0.8109
	6-311+G**	$6.10\cdot10^{-10}$	0.32	1.08	0.62	0.9370	0.77	0.66	0.8623
	aug-cc-pvDZ	$1.21\cdot10^{-8}$	0.17	1.09	0.63	0.8891	0.71	0.69	0.8670
BLYP	6-31G*	$1.17\cdot10^{-8}$	0.23	1.05	0.46	0.9193	0.57	0.49	0.9085
	6-31+G**	$1.56\cdot10^{-8}$	0.33	1.06	0.48	0.9049	0.68	0.50	0.8949
	6-311+G**	$1.11\cdot10^{-8}$	0.60	1.01	0.60	0.8819	0.69	0.61	0.8814
	aug-cc-pvDZ	$7.19\cdot10^{-9}$	0.33	1.05	0.54	0.9080	0.64	0.56	0.9019
PBE0	6-31G*	$2.54\cdot10^{-11}$	0.01	1.11	0.54	0.8864	0.79	0.71	0.8058
	6-31+G**	$1.69\cdot10^{-8}$	0.01	1.12	0.57	0.8697	0.74	0.72	0.7963
	6-311+G**	$6.34\cdot10^{-10}$	0.05	1.12	0.64	0.8545	0.75	0.74	0.8039
	aug-cc-pvDZ	$4.19\cdot10^{-11}$	0.01	1.12	0.57	0.8950	0.72	0.70	0.8375
B3LYP	6-31G*	$1.18\cdot10^{-8}$	0.03	1.09	0.51	0.8959	0.67	0.61	0.8508
	6-31+G**	$1.52\cdot10^{-8}$	0.01	1.11	0.53	0.8814	0.72	0.63	0.8316
	6-311+G**	$3.86\cdot10^{-10}$	0.08	1.11	0.58	0.8705	0.75	0.65	0.8380
	aug-cc-pvDZ	$5.66\cdot10^{-10}$	0.01	1.10	0.60	0.8791	0.69	0.69	0.8431
M06	6-31G*	$1.11\cdot10^{-13}$	$7.39\cdot10^{-13}$	1.14	0.61	0.8402	0.91	0.80	0.7205
	6-31+G**	$2.85\cdot10^{-11}$	0.01	1.16	0.56	0.8525	0.96	0.75	0.7376
	6-311+G**	$6.81\cdot10^{-11}$	0.01	1.16	0.58	0.8396	0.95	0.75	0.7360
	aug-cc-pvDZ	$6.21\cdot10^{-11}$	0.01	1.15	0.63	0.8507	0.90	0.79	0.7692
M06-2X	6-31G*	$2.13\cdot10^{-8}$	0.52	1.13	0.63	0.8148	0.90	0.82	0.6877
	6-31+G**	$1.24\cdot10^{-10}$	0.01	1.16	0.62	0.8110	0.99	0.86	0.6330
	6-311+G**	$1.61\cdot10^{-11}$	0.01	1.16	0.65	0.7946	0.96	0.87	0.6306
	aug-cc-pvDZ	$5.97\cdot10^{-12}$	$1.97\cdot10^{-11}$	1.16	0.67	0.8115	0.93	0.89	0.6720
M06-HF	6-31G*	$1.32\cdot10^{-8}$	0.18	1.12	0.69	0.8213	0.85	0.87	0.7123
	6-31+G**	$1.85\cdot10^{-8}$	1.13	1.16	0.65	0.8318	0.94	0.92	0.6590
	6-311+G**	$9.82\cdot10^{-10}$	0.02	1.18	0.68	0.8104	0.95	0.94	0.6340
	aug-cc-pvDZ	$5.97\cdot10^{-5}$	$5.97\cdot10^{-5}$	1.15	0.72	0.8854	0.58	1.23	0.6655
LC-PBEPB	6-31G*	$4.32\cdot10^{-9}$	0.07	1.14	0.58	0.8516	0.99	0.76	0.7405
	6-31+G**	$8.98\cdot10^{-10}$	0.17	1.12	0.58	0.8464	1.01	0.77	0.7252
	6-311+G**	$2.78\cdot10^{-9}$	0.19	1.12	0.55	0.8659	1.04	0.73	0.7670
	aug-cc-pvDZ	$4.71\cdot10^{-9}$	0.15	1.12	0.56	0.8773	1.01	0.75	0.7785
CAM-B3LYP	6-31G*	$5.81\cdot10^{-9}$	0.09	1.12	0.60	0.8665	0.80	0.87	0.7184
	6-31+G**	$3.40\cdot10^{-9}$	0.16	1.13	0.55	0.8769	0.94	0.87	0.6960
	6-311+G**	$8.28\cdot10^{-9}$	0.12	1.14	0.59	0.8586	0.95	0.87	0.6937
	aug-cc-pvDZ	$2.36\cdot10^{-9}$	0.10	1.13	0.58	0.8875	0.86	0.87	0.7475
ωB97X	6-31G*	$2.29\cdot10^{-10}$	$5.0\cdot10^{-4}$	1.05	0.53	0.8695	0.74	0.69	0.7752
	6-31+G**	$5.0\cdot10^{-4}$	$5.0\cdot10^{-4}$	1.15	0.51	0.8607	0.90	0.73	0.7207
	6-311+G**	$3.19\cdot10^{-10}$	$3.40\cdot10^{-10}$	1.15	0.46	0.8874	0.91	0.68	0.7517
	aug-cc-pvDZ	$3.44\cdot10^{-10}$	$4.61\cdot10^{-10}$	1.14	0.49	0.8924	0.84	0.71	0.7786
PBE-D2	6-31G*	0.1593	0.1819	1.09	0.60	0.8377	0.80	0.71	0.7735
	6-31+G**	$2.04\cdot10^{-8}$	0.25	1.11	0.58	0.8392	0.91	0.69	0.7707
	6-311+G**	$2.05\cdot10^{-8}$	0.29	1.11	0.61	0.8465	0.90	0.69	0.8031
	aug-cc-pvDZ	$1.12\cdot10^{-8}$	0.20	1.11	0.62	0.8549	0.82	0.71	0.8140
B3LYP-D2	6-31G*	$6.61\cdot10^{-11}$	0.01	1.13	0.59	0.7945	0.89	0.76	0.6546
	6-31+G**	$1.23\cdot10^{-8}$	0.11	1.14	0.65	0.7659	0.96	0.79	0.6546
	6-311+G**	$1.75\cdot10^{-8}$	0.09	1.15	0.59	0.8102	0.97	0.73	0.7090
	aug-cc-pvDZ	0.02	0.02	1.14	0.61	0.8183	0.91	0.75	0.7226
ωB97XD	6-31G*	0.05	0.05	1.12	0.63	0.7745	0.84	0.78	0.6595
	6-31+G**	$1.27\cdot10^{-11}$	0.01	1.14	0.54	0.8261	0.91	0.74	0.7790
	6-311+G**	$4.19\cdot10^{-10}$	$9.34\cdot10^{-10}$	1.16	0.50	0.8499	0.93	0.70	0.8062
	aug-cc-pvDZ	$2.18\cdot10^{-13}$	$7.52\cdot10^{-13}$	1.13	0.53	0.8618	0.85	0.72	0.8481
HF	6-31G*	0.29	0.29	1.03	0.46	0.8882	0.63	0.50	0.6308
	6-31+G**	$1.08\cdot10^{-8}$	0.18	1.08	0.44	0.8454	0.69	0.49	0.8562
	6-311+G**	$8.31\cdot10^{-9}$	0.05	1.10	0.38	0.9117	0.73	0.46	0.8699
	aug-cc-pvDZ	$4.04\cdot10^{-9}$	0.02	1.10	0.37	0.9280	0.71	0.46	0.8857
MP2	6-31G*	$1.34\cdot10^{-8}$	0.05	1.08	0.36	0.9179	0.80	0.44	0.8775
	6-31+G**	$8.77\cdot10^{-11}$	0.01	1.11	0.36	0.9072	0.89	0.47	0.8432
	6-311+G**	$9.37\cdot10^{-11}$	$4.30\cdot10^{-4}$	1.10	0.36	0.8692	0.87	0.42	0.8560
	aug-cc-pvDZ	$5.77\cdot10^{-15}$	$9.45\cdot10^{-12}$	1.08	0.42	0.8758	0.77	0.48	0.8399

Figure Captions.

Fig. 1. Chemical structure for the ions involved in the selected family of ionic liquids.

Fig. 2. a) Average values of cation-anion binding energies ($\Delta E_{IL,av}$) calculated at each theoretical level; b) RMSD of cation-anion binding energies; c) Effect of the functional over ionic liquid geometries.

Fig. 3. Average values of cation-XO_2 binding energies ($\Delta E_{cat\text{-}XO2,av}$): a) $XO_2 = CO_2$; b) $XO_2 = SO_2$

Fig. 4. RMSD of cation-XO_2 binding energies: a) $XO_2 = CO_2$; b) $XO_2 = SO_2$.

Fig. 5. Average values of anion-XO_2 binding energies ($\Delta E_{ani\text{-}XO2,av}$): a) $XO_2 = CO_2$; b) $XO_2 = SO_2$

Fig. 6. RMSD of anion-XO_2 binding energies: a) $XO_2 = CO_2$; b) $XO_2 = SO_2$.

Fig. 7. RMSD of ion-XO_2 binding energies

Fig. 8. Average values of IL-XO_2 binding energies estimated according to Eq. 2 ($\Delta E_{cat\text{-}ani\text{-}XO2,av}$): a) $XO_2 = CO_2$; b) $XO_2 = SO_2$

Fig. 9. RMSD of IL-XO_2 binding energies estimated according to Eq. 2: a) $XO_2 = CO_2$; b) $XO_2 = SO_2$.

Fig. 10. Average values of IL-XO_2 binding energies estimated according to Eq. 3 ($\Delta E_{IL\text{-}XO2,av}$): a) $XO_2 = CO_2$; b) $XO_2 = SO_2$

Fig. 11. RMSD of IL-XO_2 binding energies estimated according to Eq. 3: a) $XO_2 = CO_2$; b) $XO_2 = SO_2$.

Fig. 12. RMSD of $\Delta E_{IL\text{-}XO2}$ binding energies

Fig. 13. Effect of the functional over IL-XO_2 geometries: a) $XO_2 = CO_2$; b) $XO_2 = SO_2$.

Fig. 14. ΔE_{IL} (up), $\Delta E_{IL\text{-}CO2}$ (middle) and $\Delta E_{IL\text{-}SO2}$ (bottom) for studied ILs calculated for different methods in combination with aug-cc-pvDZ basis set.

Fig. 15. $\Delta E_{IL\text{-}CO2}$ (green) and $\Delta E_{IL\text{-}SO2}$ (red) for studied ILs calculated at ωB97XD/6-31+G** theoretical level.

Cations

1-Ethyl-3-methylimidazolium $[EMIM]^+$

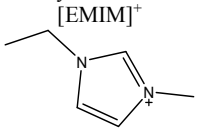

1,3-Dimethylimidazolium $[DMIM]^+$

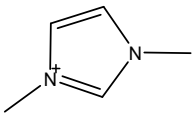

1-hexyl-3-methylimidazolium $[HMIM]^+$

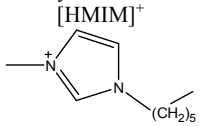

1-Methyl-3-octylimidazolium $[OMIM]^+$

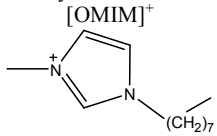

1-butyl-3-methylimidazolium $[BMIM]^+$

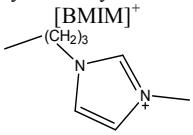

1-methyl-3-propylimidazolium $[MPIm]^+$

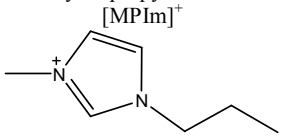

1-Allyl-3-methylimidazolium $[AMIM]^+$

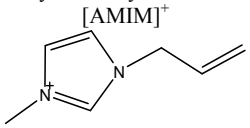

1-Butyl-2,3-dimethylimidazolium $[BDMIM]^+$

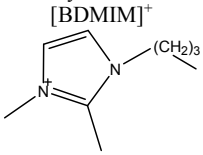

1,2-Dimethyl-3-propylimidazolium $[DMPIm]^+$

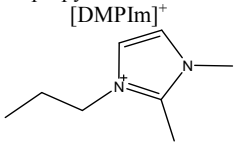

1-Methyl-1-propylpyrrolidinium $[MPPyr]^+$

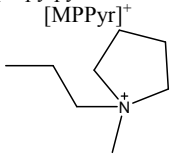

1-Butyl-1-methylpyrrolidinium $[BMPyr]^+$

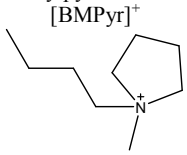

1-Butylpyridinium $[BPy]^+$

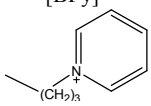

1-Butyl-3-methylpyridinium $[B3MPy]^+$

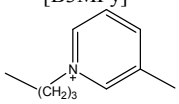

1-Butyl-4-methylpyridinium. $[B4MPy]^+$

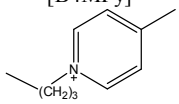

1-Methyl-1-propylpiperidinium $[MPPipe]_+$

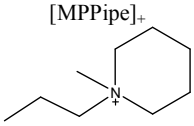

Choline $[CH]^+$

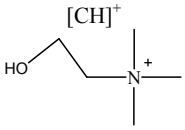

Ethylammonium $[EtNH_3]^+$

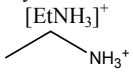

Triethylsulfonium $[Et_3S]^+$

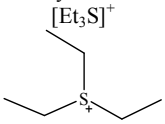

Anions

Tetrafluoroborate $[BF_4]^-$

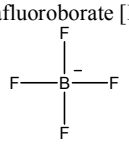

Diethylphosphate $[Et_2PO_4]^-$

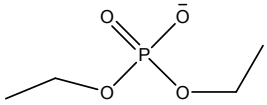

bis[(trifluoromethyl)sulfonyl]imide $[NTf_2]^-$

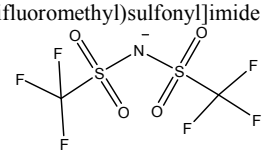

Hexafluorophosphate $[PF_6]^-$

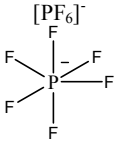

Dimethylphosphate $[Me_2PO_4]^-$

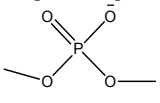

Triflate $[SO_3CF_3]^-$

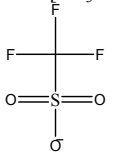

Dicyanamide $[DCA]^-$

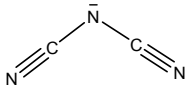

Acetate $[Ac]^-$

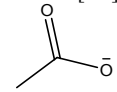

Dihydrogenphosphate $[H_2PO_4]^-$

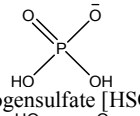

Thiocianate $[SCN]^-$

Cloride $[Cl]^-$

Bromide $[Br]^-$

Iodide $[I]^-$

Nitrate $[NO_3]^-$

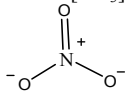

Hidrogensulfate $[HSO_4]^-$

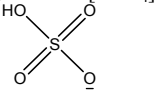

Ethylsulfate $[EtSO_4]^-$

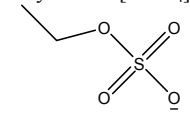

Fig. 1

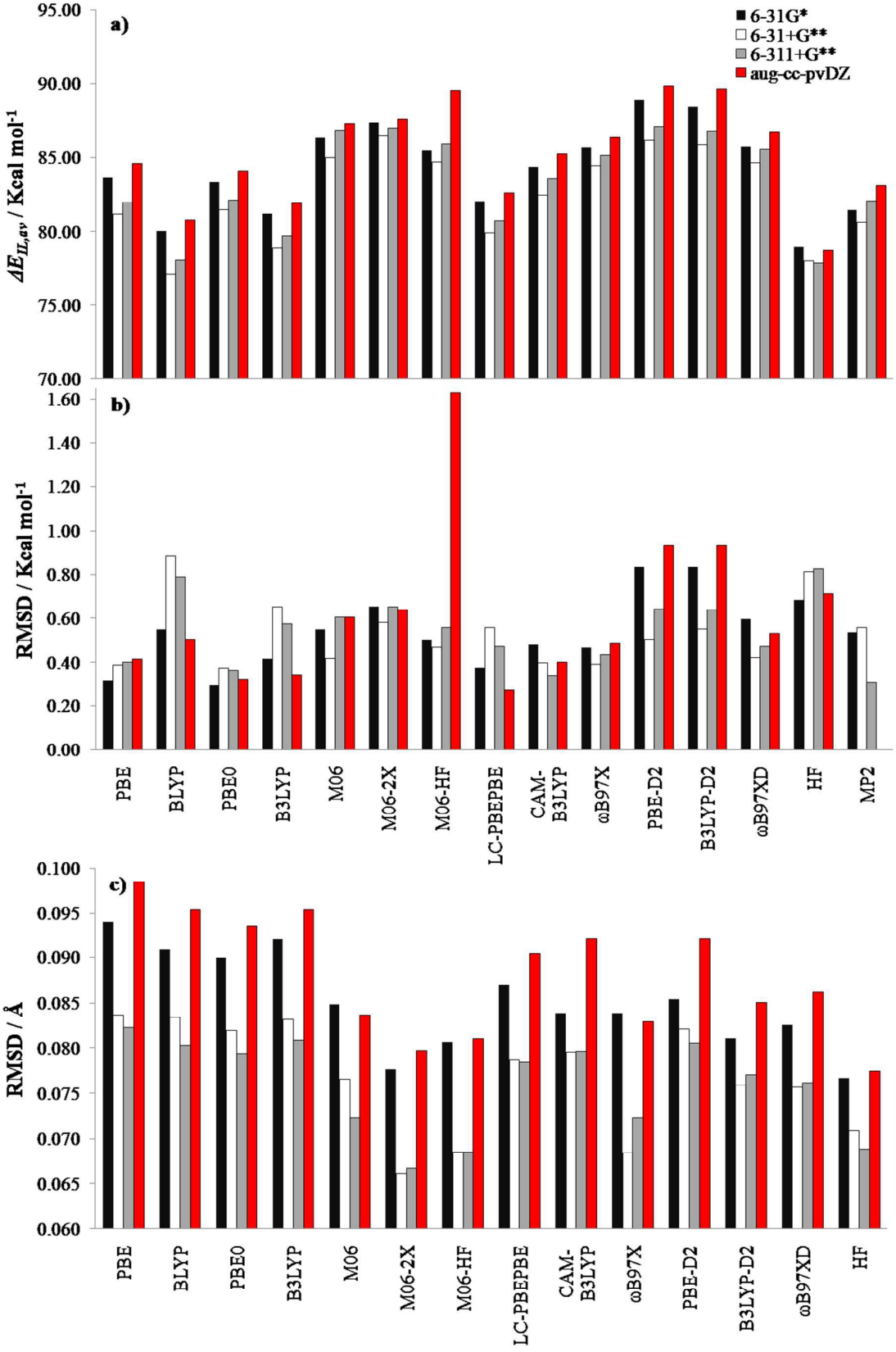

Fig. 2

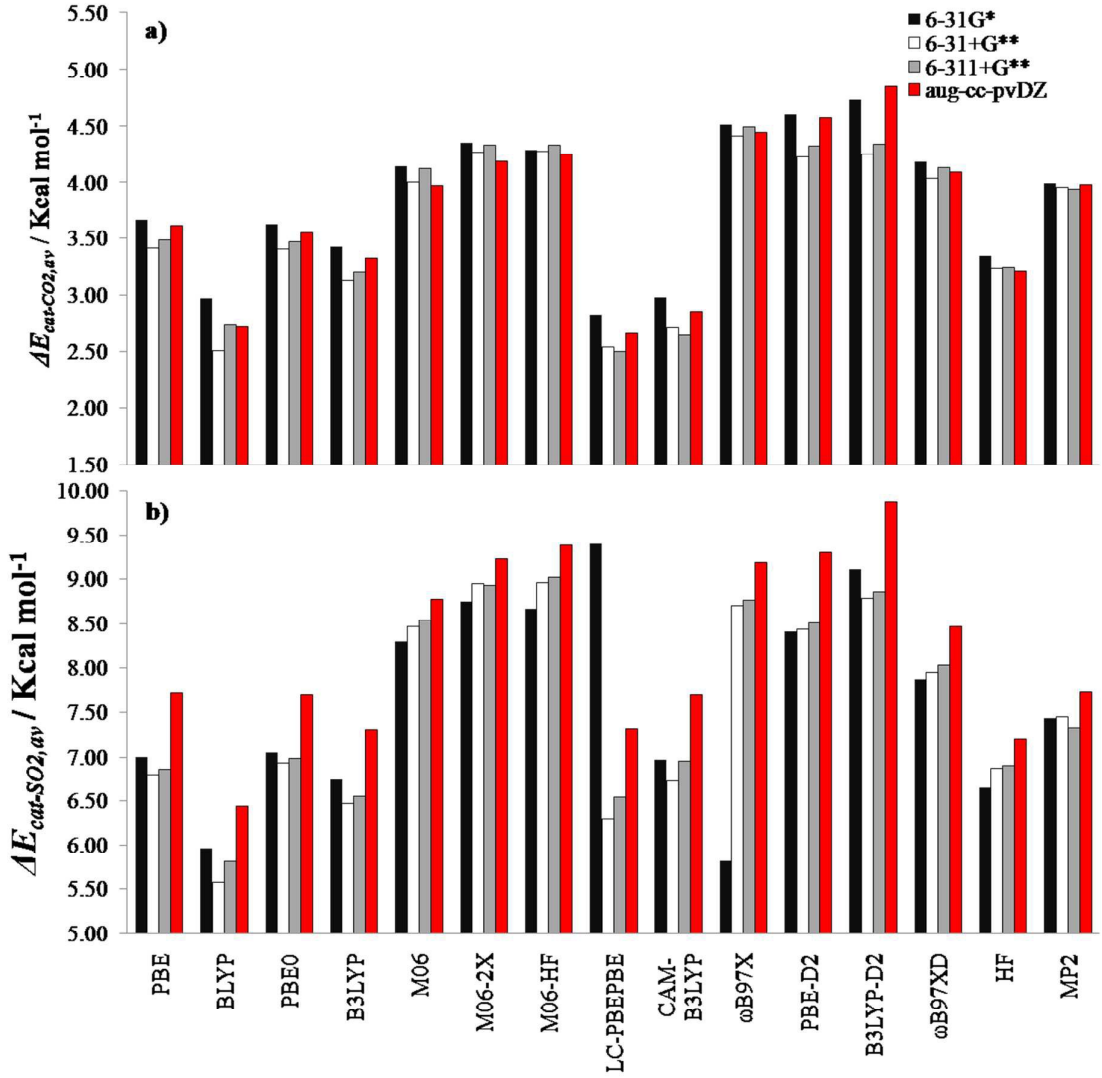

Fig. 3

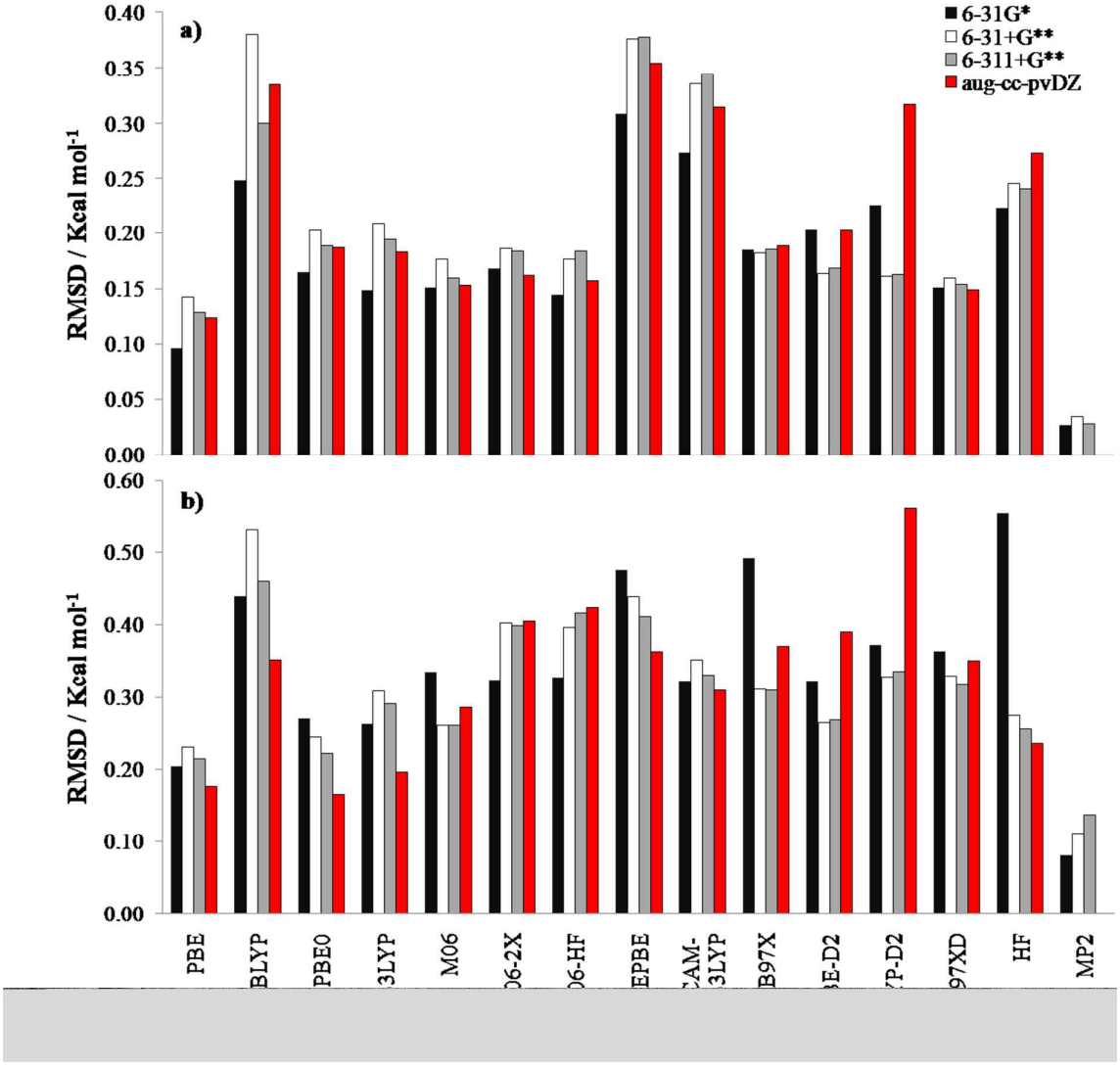

Fig. 4

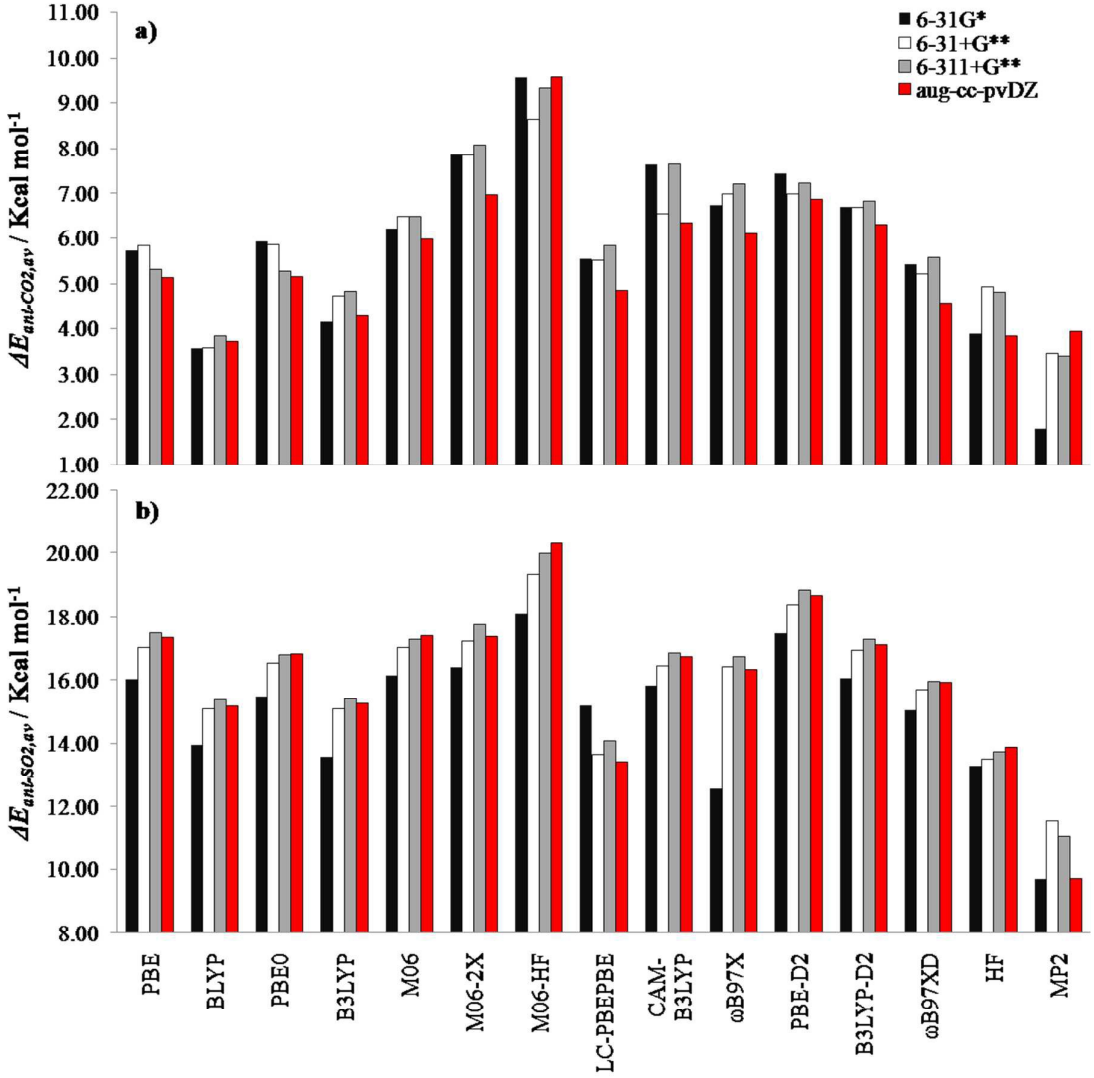

Fig. 5

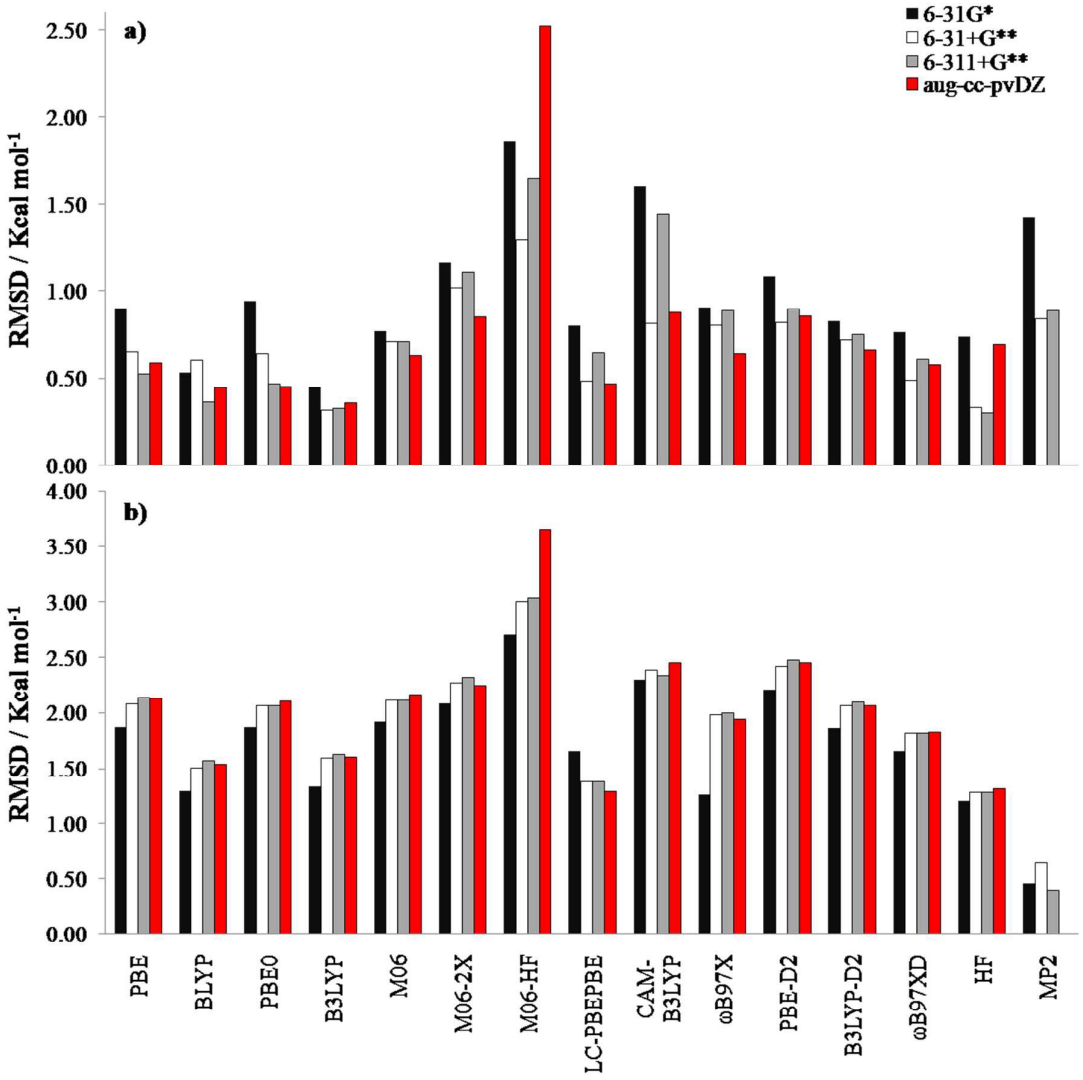

Fig. 6

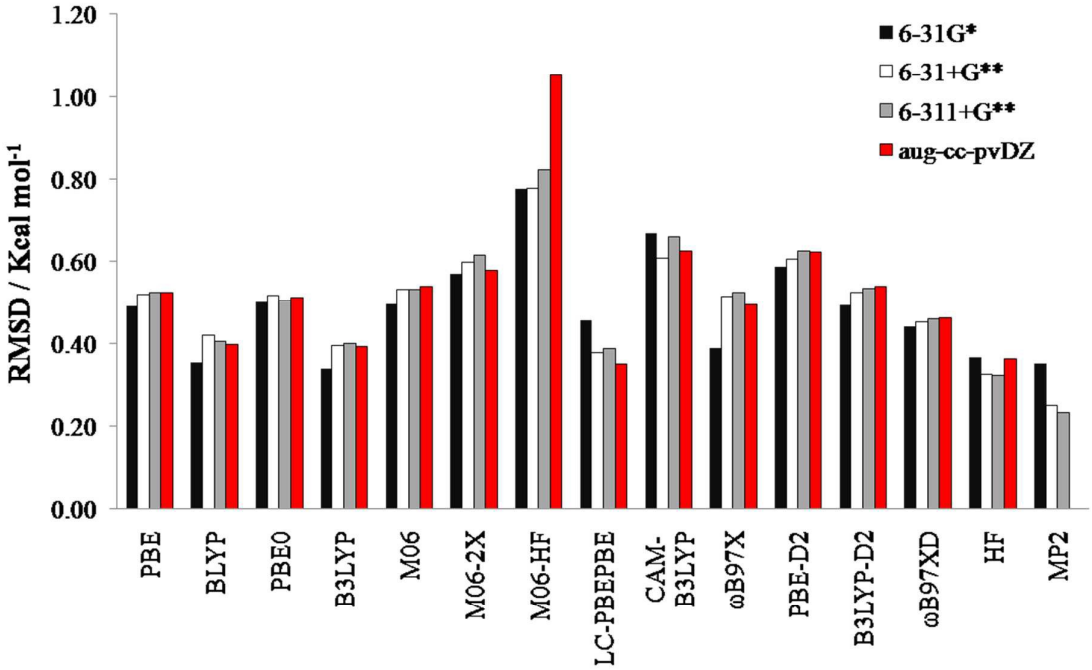

Fig. 7

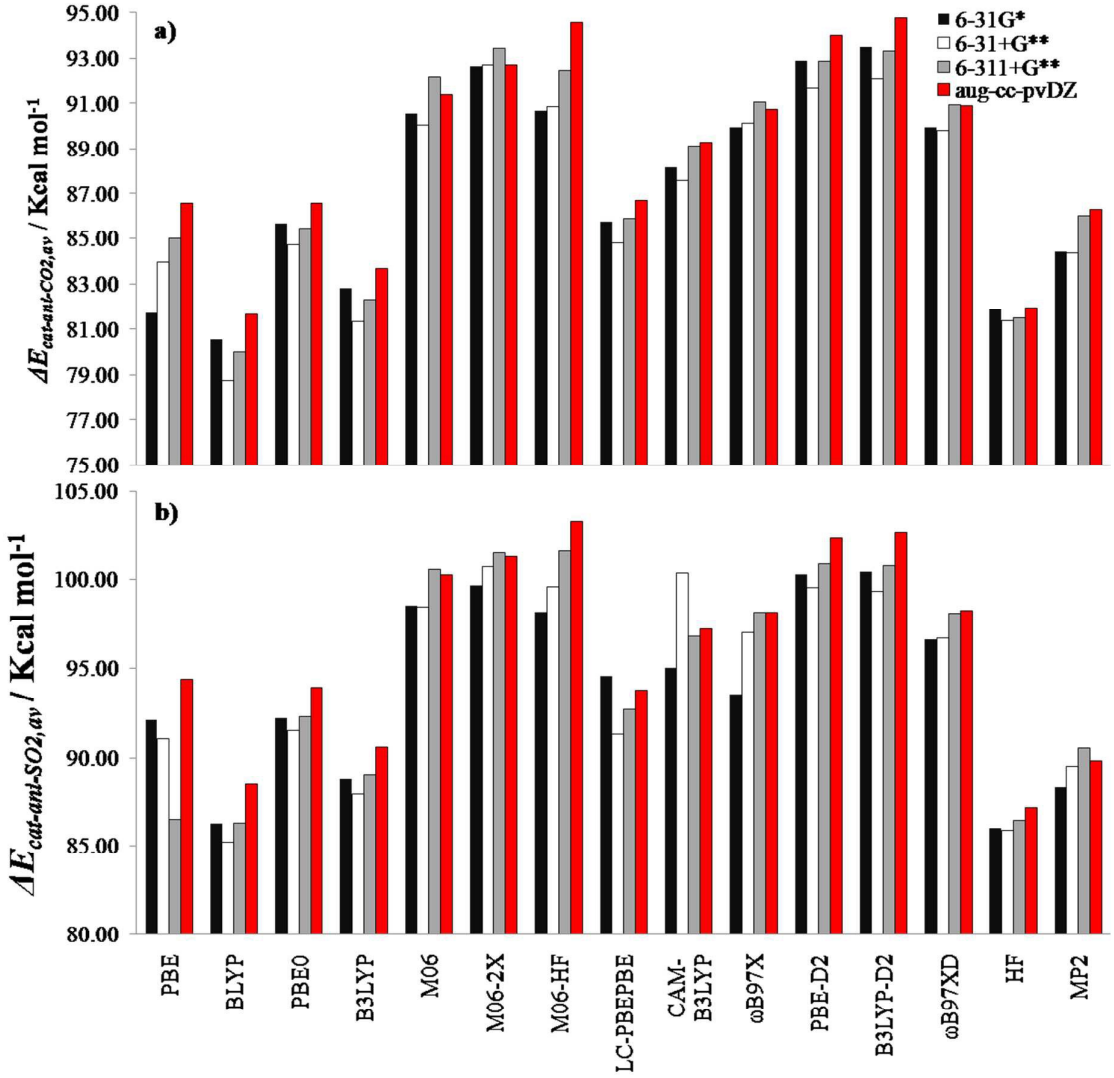

Fig. 8

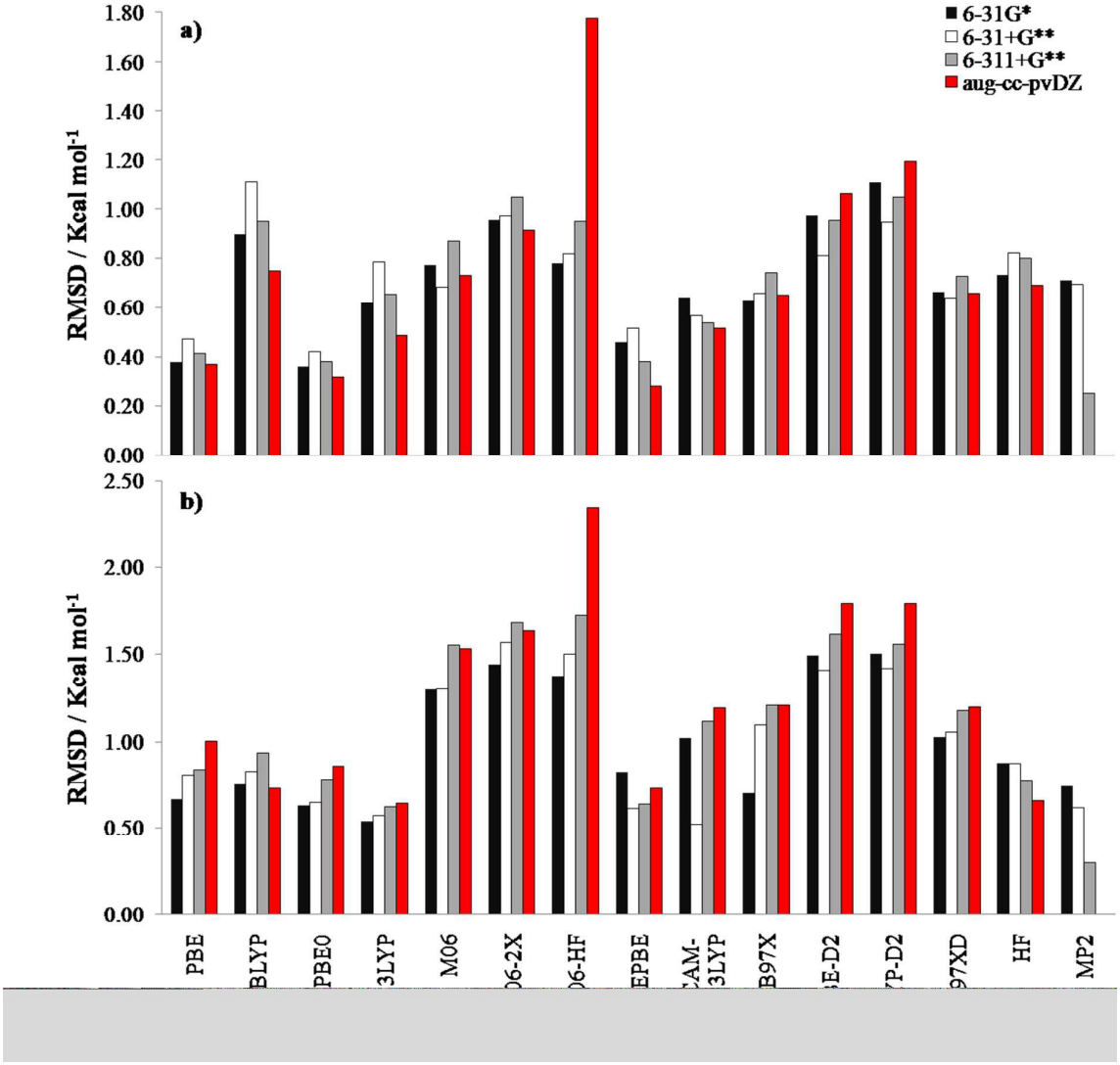

Fig. 9

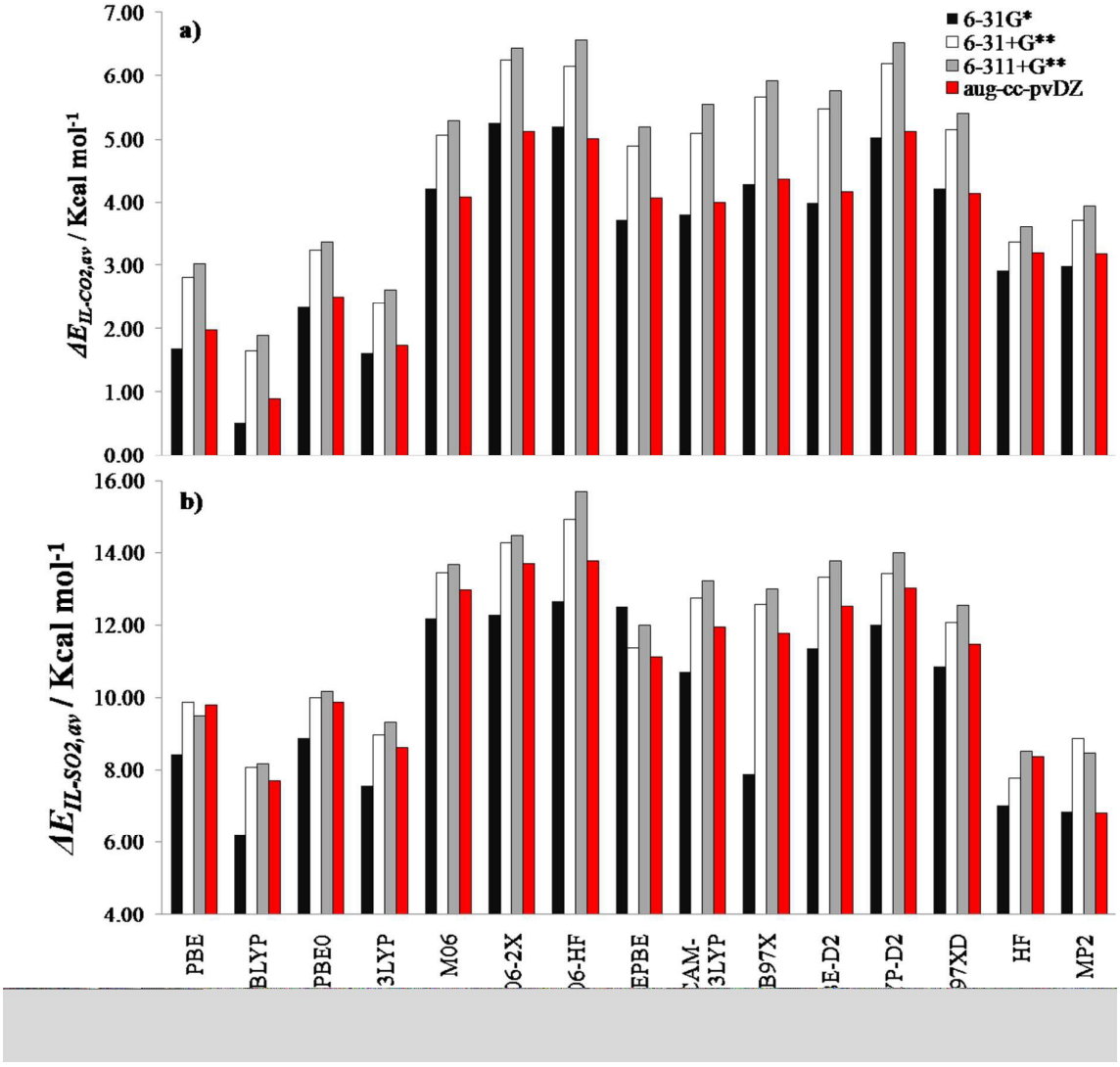

Fig. 10

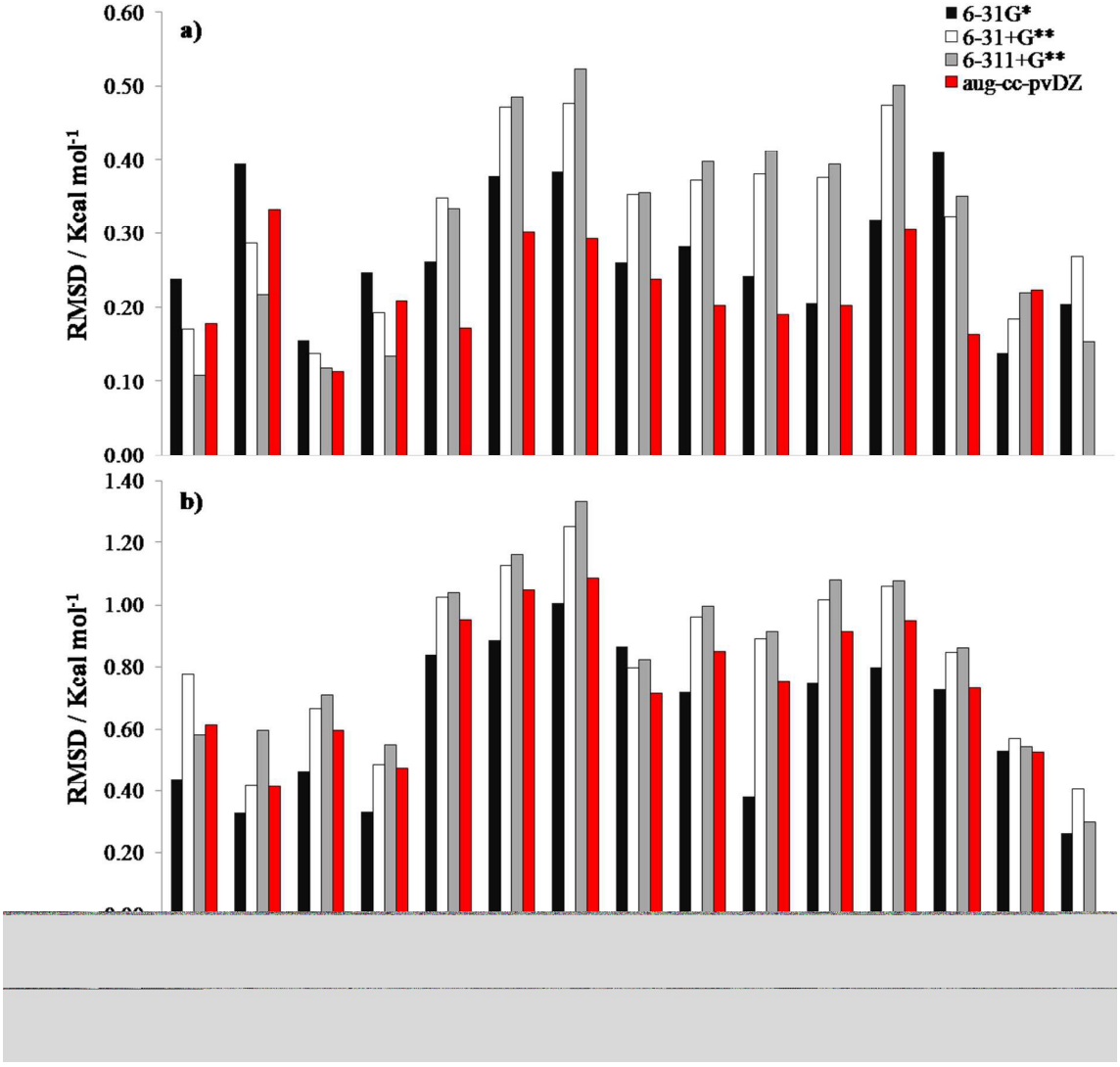

Fig. 11

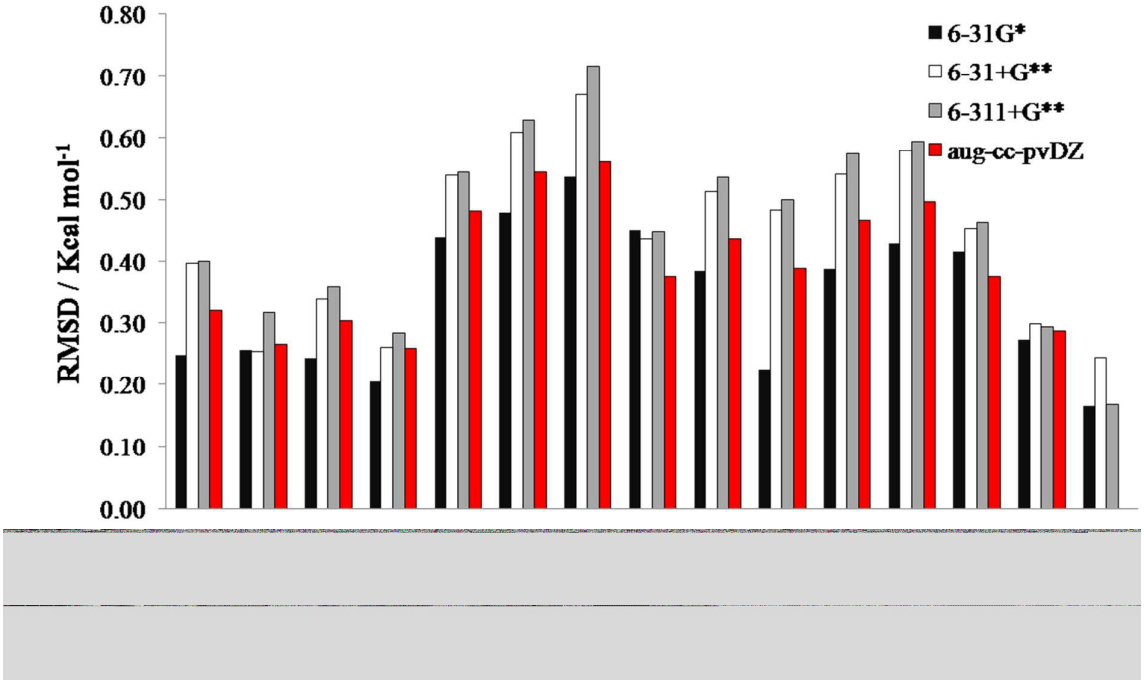

Fig. 12

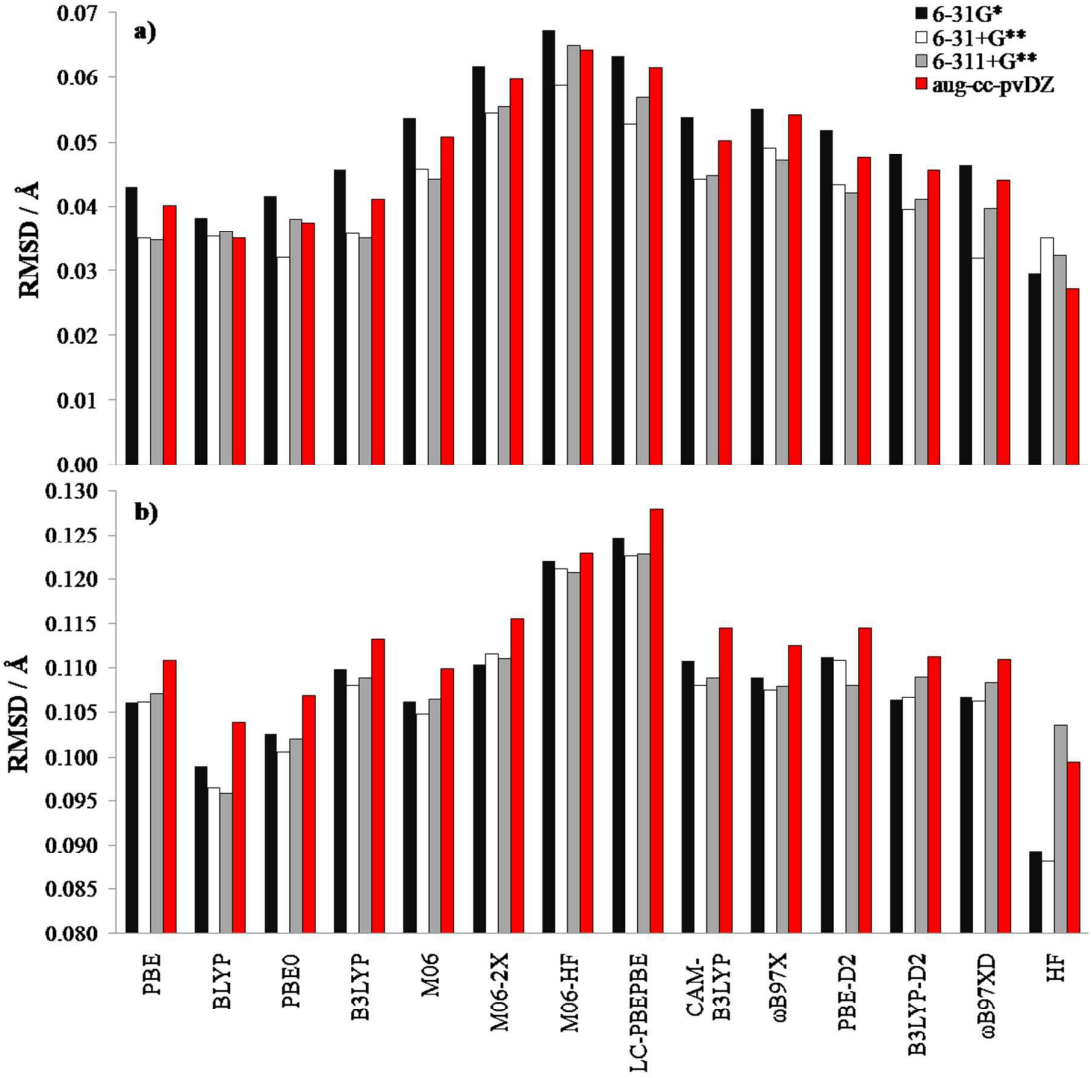

Fig. 13

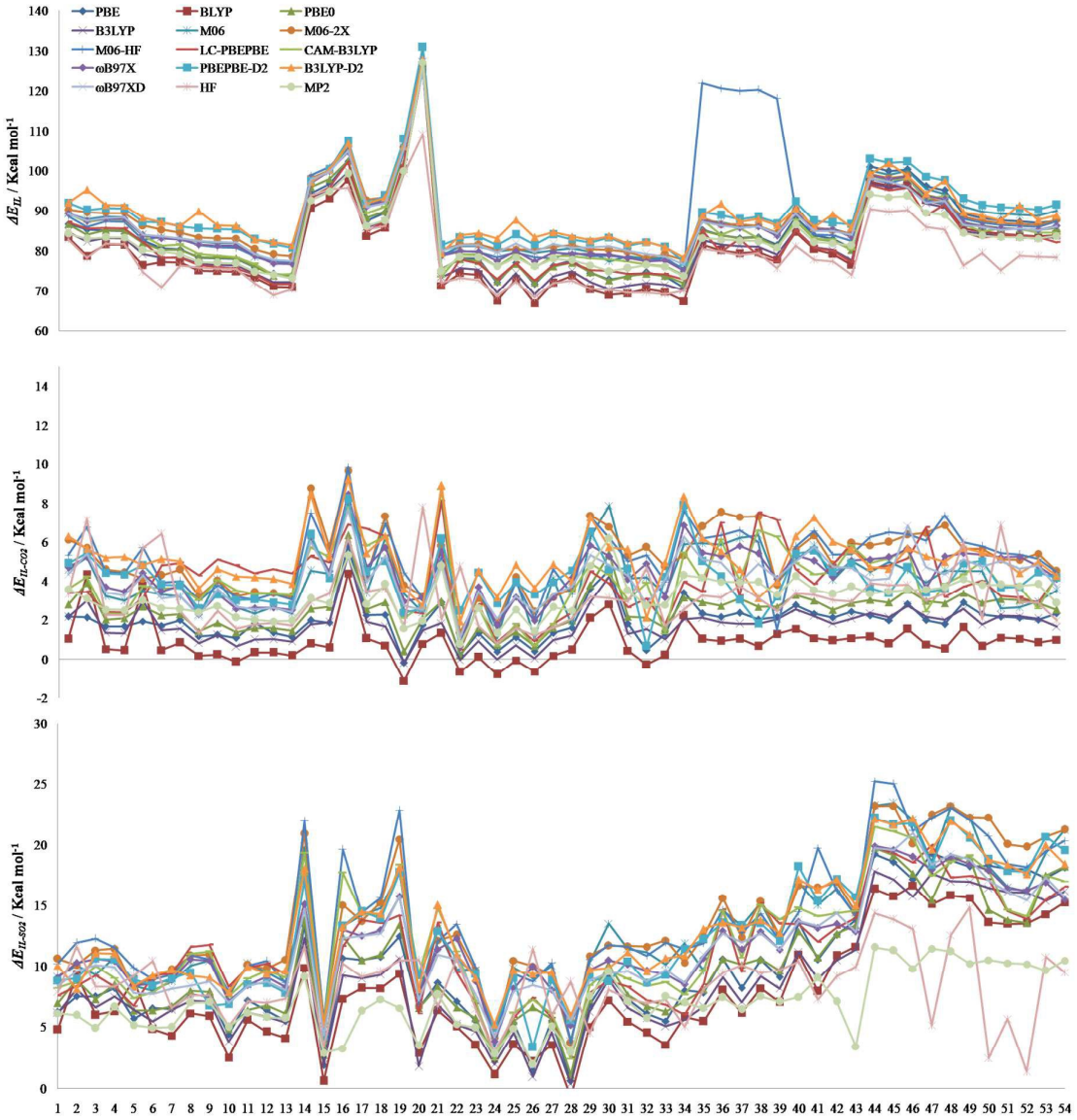

Fig. 14

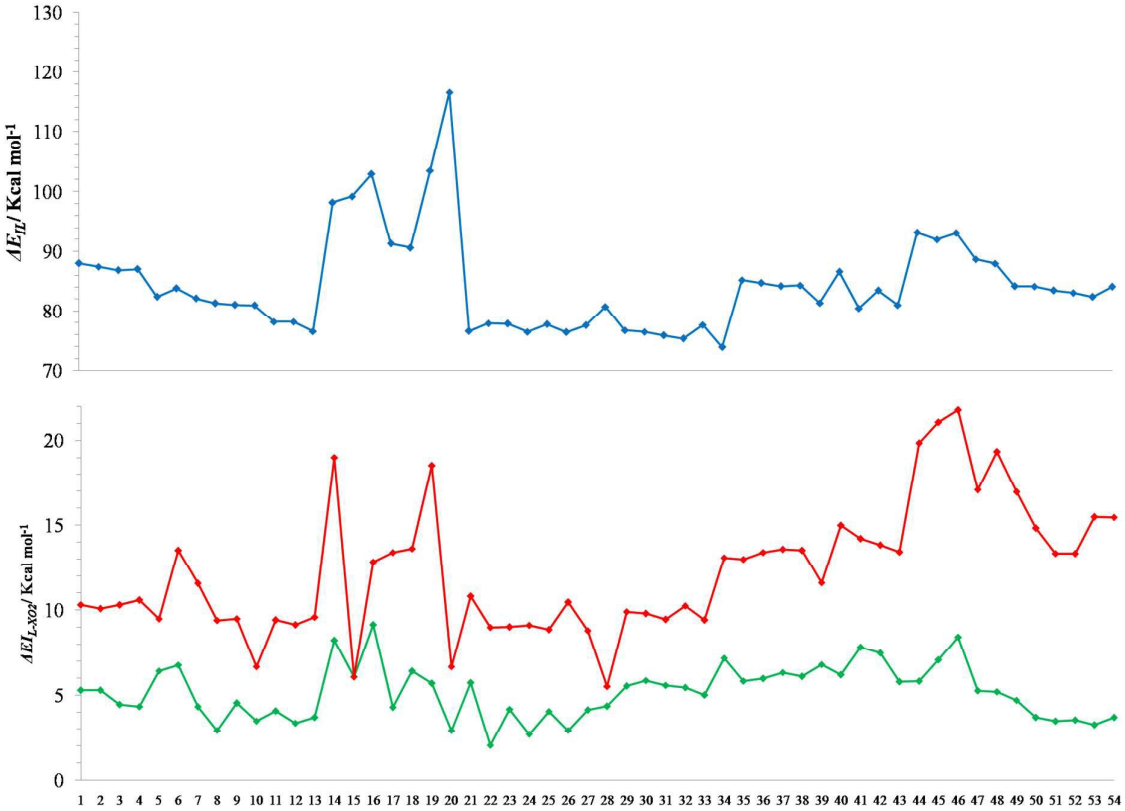

Fig. 15